8-2024

I’m a Forest, Not a Saltmarsh, Captain: Carbon and Sap Flow Dynamics in Coastal Forested Wetlands of the Southeastern United States

Chris Shipway
cjshipw@clemson.edu

I'M A FOREST, NOT A SALTMARSH, CAPTAIN; CARBON AND SAP FLOW DYNAMICS IN COASTAL FORESTED WETLANDS OF THE SOUTHEASTERN UNITED STATES

A Thesis
Presented to
the Graduate School of
Clemson University

In Partial Fulfillment
of the Requirements for the Degree
Master of Science
Forest Resources

---

by
Christopher James Shipway
August 2024

Accepted by:
Dr. Stefanie Whitmire, Committee Chair
Dr. William Conner
Dr. Jamie Duberstein
Dr. Skip Van Bloem

ABSTRACT

Coastal forested wetlands are identified as some of the highest-priority ecosystems for climate change mitigation. Here, we present two studies conducted in these unique ecosystems.

The first assessed changes in aboveground vegetative C stocks along the estuarine-riverine gradients of the Winyah Bay in South Carolina and the Savannah River in Georgia, using a space-for-time substitution to increase understanding of the impacts to upper estuarine forested wetlands from relative sea level rise. Standing C stocks on the Savannah River averaged 183.6 Mg C ha^{-1}, while sites on the Winyah system averaged 162.3 Mg C ha^{-1}. The largest aboveground C pools were found at sites furthest upriver, decreasing downstream as salinity rose. These data, alongside predicted sea-level rise suggest a marked decrease in future aboveground C stocks in forested wetlands situated in and around tidal estuaries.

Our second study investigated the radial and azimuthal patterns of sap flow in species (baldcypress and water tupelo) common to the freshwater swamps of the southeastern US, suspecting that these diverse species may exhibit similar sap flow patterns under permanently flooded conditions. Granier-style thermal dissipation probes were used to measure daytime sap flux at 15 mm and 25 mm depths into the active xylem of both species to assess radial patterning and at each cardinal direction on the bole of each species to assess azimuthal patterning. Analysis of sub-daily time series data found significant ($p < 0.05$) effects on sap flux by time of day, month, species, and depth. We did not find any differences between the two depths with water tupelo ($p > 0.5$), but

average baldcypress flux rates at 15 mm were significantly higher than those at 25 mm ($p < 0.0001$). Azimuthal patterns were not detected for either species, contradicting previous studies. This study supports the treatment of azimuthal sap flow variation as a random variable rather than one with predictable directionality, and demonstrates that common radial sap flow patterns may not be generalizable across diverse environmental settings. Because our study found temporal variation in sap flux rates, the inclusion of these temporal factors could improve modeling estimates of individual tree water use.

DEDICATION

I would like to dedicate this thesis to my father, John Shipway. Dad-o; studies of your patience in getting me through those early math classes could fill a thousand theses. Throughout my life your unwavering support has been my foundation, and your guidance will always be my north star.

ACKNOWLEDGMENTS

I would like to acknowledge all the people who have kept me sane through this project, beginning with my mother, Lydia Shipway; without you raising me this way I would never have had the imagination, courage, or confidence to even begin. I also thank my little brother Muffin, simultaneously my greatest supporter and wittiest critic. All four of my advisors have provided incredible support; whether providing hurricane shelter or a thanksgiving table, they have all gone above and beyond to welcome me into their homes and families, for which I will always be grateful. I would like to thank my friends for the moments of connection, large and small, despite the demands of a student's schedule which have not made me the easiest friend to hold onto. Michael Kline and Brian Williams both provided technical and field support for which I am eternally grateful. Samantha Elie has provided infinite support, inspiration, and feedback without which this project would not be half of what it is today. Finally, I would like to thank Kelsea McBrayer and Nymane, for taking such good care of me these last five years.

Access to the beautiful Hobcaw Barony was provided by the Belle W. Baruch Foundation, without which these studies would not have been possible. I am thankful for the research assistantship provided by the Savannah District US Army Corps of Engineers under Cooperative Agreement W912HZ-19-2-0007, coordinated by the Piedmont-South Atlantic Coast Cooperative Ecosystem Studies Unit.

TABLE OF CONTENTS

Page

TITLE PAGE i

ABSTRACT ii

DEDICATION iv

ACKNOWLEDGMENTS v

LIST OF TABLES viii

LIST OF FIGURES ix

CHAPTER

I. THE BREATH AND BREADTH OF GHOSTS; BIOMASS DYNAMICS AND TRANSPIRATION ESTIMATION IN ESTUARINE FORESTED WETLANDS 1

1.1 Overview; scope, context, and connection 1
1.2 Understanding C; from the globe to the ghosts 4
1.3 Understanding Sap Flow; the breath of the earth 13
1.4 Conclusion 23

II. ABOVEGROUND CARBON STOCKS ACROSS A HYDROLOGICAL GRADIENT: GHOST FORESTS TO NON-TIDAL FRESHWATER FORESTED WETLANDS 24

2.1 Introduction 24
2.2 Methods 27
2.3 Results 33
2.4 Discussion 42
2.5 Conclusion 47

III. RADIAL AND AZIMUTHAL ATTENUATION IN BALDCYPRESS AND WATER TUPELO IN LONG HYDROPERIOD, LOW SALINITY ENVIRONMENTS OF THE SOUTHEASTERN US 49

3.1 Introduction 48
3.2 Methods 52
3.3 Results 59
3.4 Discussion 66
3.5 Conclusion 72

IV. SUMMARY AND CONCLUSIONS 73

APPENDICES 76

A: Table S1: extended species reference 77

REFERENCES 81

LIST OF TABLES

Table		Page
1.1	Globally averaged C stock density for terrestrial benchmark and “blue carbon” ecosystems	9
1.2	Rates of C burial in soils of blue carbon and benchmark ecosystems	10
1.3	Suitable applications and error sources for a variety of thermometric sapflow methods	16
2.1	C stocks at study sites along the Winyah and Savannah rivers	36
2.2	Tree species contributions to standing biomass stocks	37
2.3	Herbaceous species contributions to standing biomass stocks	38
2.4	Comparison of codominant tree C values from Krauss (2018) and the current work	44
3.1	Average salinity measurements across the study duration in Strawberry Swamp, South Carolina, USA	59
3.2	Radial patterns observed in archetypal non-porous species and baldcypress (*Taxodium distichum*).	68
3.3	A non-exhaustive collection of studies reporting on the presence (or absence) and directionality of systemic azimuthal sap flow patterns.	71

LIST OF FIGURES

Figure Page

1.1 Unmodified reproduction of Figure 5.12 as originally published in Canadell et al. (2021), detailing the global carbon cycle. All values presented in Pg C yr^{-1}; yellow fluxes and pools (arrows and circles) represent historic conditions prior to the industrial revolution (1750 CE). Numbers in pink circles represent net changes in these stocks due to anthropogenic influence since 1750, while pink arrows represent average annual anthropogenic fluxes from 2010 – 2019. See full citations and original caption at URL: https://www.ipcc.ch/report/ar6/wg1/figures/chapter-5/figure-5-12. 5

1.2 Reproduction of Figure 1 as originally published by Adame et al. (2024), depicting archetypal UEFW using (a) Australian Casuarina or Melaleuca forests or (b) cypress forests of the southeastern United States and the environmental and elevational distributions (c) along which these “other wetlands” are found. HAT: highest astronomical tide. MSL: mean sea level. URL: https://academic.oup.com/view-large/figure/444118846/biae007fig1.jpg. 12

1.3 Reproductions of (a) Steppe et al. (2010) Figure 1 (modified), and (b) Lascano et al. (2016) Figure 1 (unmodified), depicting archetypal methods from each of the TSM families. Methods depicted in (a) include; thermal dissipation (*e.g.*, Granier, 1987) in the top left, heat field deformation (*e.g.*, Nadezhdina et al., 1998) in the bottom left, and compensation heat pulse heat pulse (*e.g.*, Steppe et al., 2010) on the right. The heat balance family in (b) is represented by the stem heat balance method adapted from its original patent (Van Bavel & Van Bavel, 1993). URL (figure 1a): https://ars.els-cdn.com/content/image/1-s2.0-S0168192310001000-gr1.jpg. URL (figure 1b): https://www.scirp.org/journal/paperinformation?paperid=70680#f1. 15

2.1 Site locations within the southeastern Atlantic coast of the United States including the Savannah River and Winyah Bay systems in Georgia and South Carolina, respectively. 28

2.2 Water level patterns vary across the estuarine gradient of the systems, being characterized as either low-frequency, high-magnitude (left) or semidiurnal (right) flood patterns. Note that the two hydrographs show different temporal scales on the x-axes, but the same meter scale on the y-axes. 34

2.3 Observed aboveground C (Mg ha^{-1}) by estuary position. 40

2.4 (Top) Tree carbon (C) in Megagrams per hectare by river position. (Bottom) Percent contribution of each biomass pool to the given plot's total C, barring live mature trees. 42

3.1 Located on Hobcaw Barony in Georgetown County, SC, the study took place in a cypress-tupelo swamp typical of the region. Sap flow and weather station locations remained identical across both deployments. 53

3.2 Thermal Dissipation probes as deployed in the field in 2020. 4 probes were deployed at 90-degree angles around the tree, aligned with cardinal headings. Mylar shielding was used to protect the probes from rainfall and sunlight which could affect temperature readings. 55

3.3 Js rates (g m^{-2} sec^{-1}) of water tupelo (*Nyssa aquatica*) and baldcypress (*Taxodium distichum*) trees in Strawberry Swamp. Subset analyses reveal no difference by depth in water tupelo, but differences by depth were significant in baldcypress. 61

3.4 Js (g m^{-2} sec^{-1}) patterns of water tupelo (*Nyssa aquatica*) and baldcypress (*Taxodium distichum*) from April to September, at 15- and 25-mm sapwood depths. Error bands represent a 95% confidence interval. Note that the sample size for baldcypress 25 mm depth is only 2, and thus is prone to greater error. 62

3.5 Monthly variation in Js (g m^{-2} sec^{-1}) response of water tupelo (*Nyssa aquatica*) and baldcypress (*Taxodium distichum*) trees in Strawberry Swamp. Error bands represent 95% confidence intervals. Letters represent differences according to Tukey's HSD test of subset model LSM estimates, where months sharing a letter are not significantly different from one another. Note that comparisons were not made between species within any given month. 63

3.6 Daily Js (g m^{-2} sec^{-1}) patterns of water tupelo (*Nyssa aquatica*) and baldcypress (*Taxodium distichum*), including observations at 15 mm and 25 mm depths. Higher overall Js rates in baldcypress appear to be driven in part by greater flows during morning and evening conditions. 64

3.7 Average daily Js (g m^{-2} sec^{-1}) patterns of baldcypress (*Taxodium distichum*) and water tupelo (*Nyssa aquatica*) measured each cardinal direction around the stem. Error bars represent the 95% confidence interval. N=10 for each combination of species and heading. Heading was not found to be a significant determinant of Js values in this sample..... 65

CHAPTER ONE

THE BREATH AND BREADTH OF GHOSTS; BIOMASS DYNAMICS AND TRANSPIRATION ESTIMATION IN ESTUARINE FORESTED WETLANDS

1.1 Overview; scope, context, and connection

Wetlands of all kinds provide incredible ecological value (Barbier et al., 2011; Smith et al., 2019) while simultaneously being among the most vulnerable systems to ongoing degradation, having lost ~ 55% of their original spatial extent (Davidson, 2014) of between 4.3 and 12.6 million km^2 (Shukla et al., 2019). Understanding the dynamics at play within these systems is therefore of critical importance to the establishment of management programs from the global to local scale (Shukla et al., 2019). In the following chapters, we report observational findings of aboveground carbon (C) stocks in Upper Estuarine Forested Wetlands (UEFW) and spatiotemporal variation of sap flow in wetland trees. Standing C stock evaluations are important in the context of ongoing climate mitigation efforts (Erb et al., 2018; Houghton et al., 2009; Shukla et al., 2019; Smith et al., 2019), and UEFW are a large (Bar-On et al., 2018; Domke et al., 2019) but poorly quantified portion of global C estimation (Houghton et al., 2009). Wetland sap flow dynamics have important implications for the estimation of tree- and stand-level water use (Dix & Aubrey, 2021b; Peters et al., 2018; Poyatos et al., 2016) in these critical systems. In this introductory chapter, we present a review of related topics that provide broader context for the more focused discussions found in chapters 2 and 3.

History and modern state of C and sap flow science

The modern understanding of global C allocation and cycling patterns, while still subject to a litany of unsolved questions (Bar-On et al., 2018; Erb et al., 2018; Friedlingstein et al., 2020; McLeod et al., 2011), is nonetheless robust enough to provide the theoretical framework for concrete and wide-ranging management decisions (Duarte et al., 2013; MacDicken, 2015; Rozendaal et al., 2022; Shukla et al., 2019) and is the result of hundreds of years of scientific investigation (Zon & Sparhawk, 1923). Recent innumerable publications summarizing the modern understanding of global C stocks include efforts led by international organizations including the IPCC (Shukla et al., 2019), the Global Climate Project (Friedlingstein et al., 2020), and the FAO (MacDicken, 2015) as well as traditional review articles (*e.g.*, Erb et al., 2018; Pan et al., 2011) which have recently reported global biomass stocks in living organisms to be around 550 Gigatons of C, of which plants make up approximately 80% (Bar-On et al., 2018). Many of these efforts are driven in whole or in part by the importance of C sequestration as an ecosystem service (Houghton et al., 2009; Krauss et al., 2018; McLeod et al., 2011; Smith et al., 2019), which is positively correlated with biomass stocks in terrestrial ecosystems (Bar-On et al., 2018; Erb et al., 2018). Nested within this body of work, "Blue Carbon" ecosystems were first described in such terms in 2009 (Laffoley, 2009; Lovelock & Duarte, 2019; Nelleman et al., 2009), driven primarily by the recognition that these ecosystems had uniquely high potential as net C sinks (Duarte et al., 2013; McLeod et al., 2011). Research interest in blue carbon ecosystems has been growing over time; one report estimated that there were 30 papers published on the subject in 2005 and

110 in 2012 (Duarte et al., 2013). Younger still is the recognition and investigation of the UEFW which compose the landward boundary of blue carbon; these novel systems have attracted a great amount of research interest in recent years (Adame et al., 2024; Kauffman et al., 2020; Lovelock & Duarte, 2019) but are not yet well established in the scientific literature.

Sap flow measurements are a well-studied component to the field of tree-water relations (Landsberg & Waring, 2017), and the methods used to quantify sap flow have been under development for more than a century (Dixon, 1914). As summarized in much greater detail by Vandegehuchte and Steppe (2013), the technology used to measure sap flow advanced greatly in the 1930s with the introduction of heat as a tracing element, and techniques have diversified rapidly ever since. The primary function of sap flow monitoring is to investigate tree water relations and physiology (Landsberg & Waring, 2017), which in turn allow the estimation of water-use budgets critical for ongoing management goals (Dix & Aubrey, 2021b; Peters et al., 2018; Poyatos et al., 2016). The standardization of methodologies regarding sensor calibration (Dix & Aubrey, 2021b), data processing (Peters et al., 2018), and accounting for within-trunk spatial variation (Poyatos et al., 2021) all remain significant hurdles contributing to high variability between and within studies. Another major source of uncertainty in the field of sap flow estimation is the impact of tree morphological characteristics such as hydraulic structure on the observed rates of sap flow (Fan et al., 2018; Kotowska et al., 2021). Despite these ongoing areas of refinement, the measurement of sap flow rates in diverse environments and taxa worldwide (da Rosa Ferraz Jardim et al., 2022; Poyatos et al., 2021) have made

informative estimates of global water transport via terrestrial transpiration feasible. Terrestrial plants are estimated to move about 45,000 km^3 of water into the atmosphere per year (Poyatos et al., 2021), which is roughly equivalent to annual river discharge worldwide (Rodell et al., 2015). Recent efforts at establishing global databases represent major strides in the field (*e.g.*, Poyatos et al., 2021) which will undoubtedly contribute to greater standardization worldwide.

1.2 Understanding C; from the globe to the ghosts

The global system of C pools and fluxes is near-infinitely complex, yet the understanding thereof is likely the most important factor in humanity's struggle with global climate change. Canadell et al. (2021), as part of the 2021 IPCC report, have presented perhaps the most comprehensive graphical summary of the global C cycle to date, with the majority of C pools and fluxes represented (Figure 1.1). Within this figure, the pools "vegetation" and "soils" account for 2,150 Pg of C in current stocks, or about 4.7% of the total. The uncertainty estimates around these estimations are large (Bar-On et al., 2018; Canadell et al., 2021; Domke et al., 2019; Erb et al., 2018; Rozendaal et al., 2022), the result of the sheer diversity in methodologies, spatial resolutions, and exogenous error sources (Bar-On et al., 2018; Erb et al., 2018). Not shown in Figure 1.1 is a relatively recently described ecosystem type which straddles the freshwater-to-marine and riverine-to-oceanic gradients; blue carbon ecosystems.

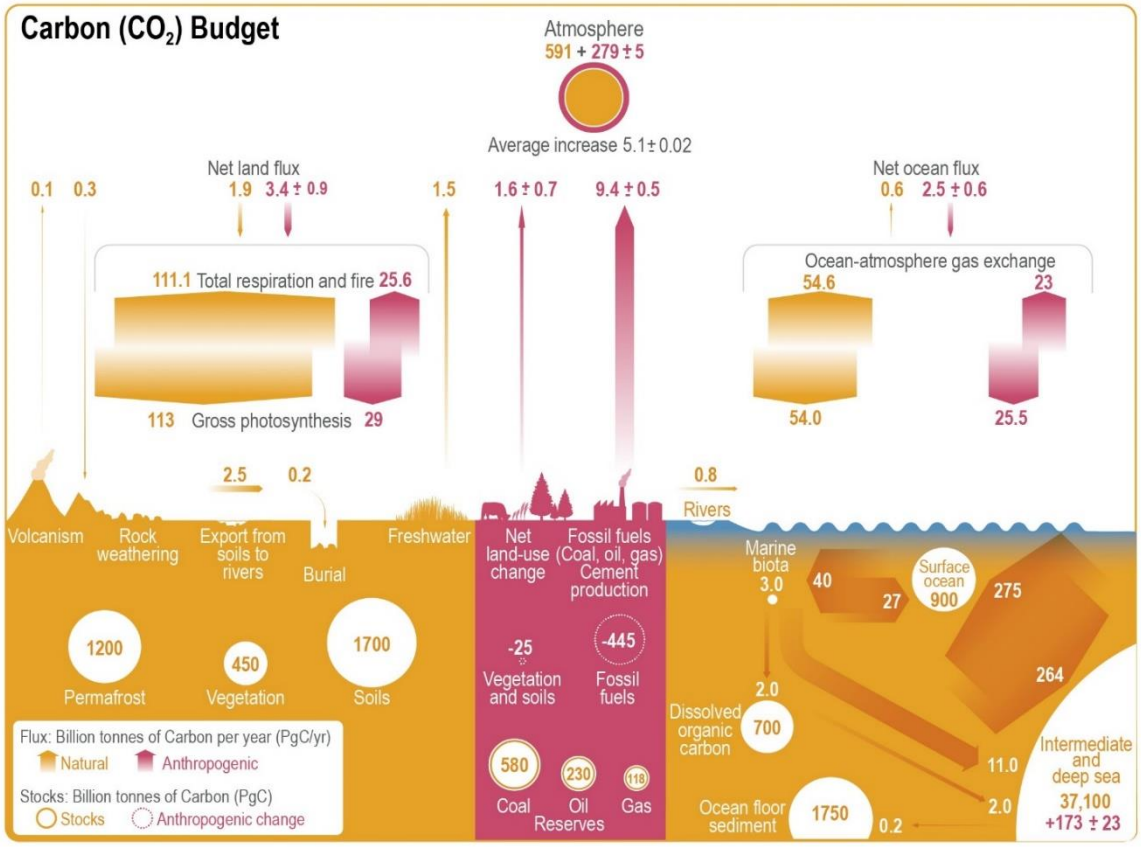

Figure 1.1. Unmodified reproduction of Figure 5.12 as originally published in Canadell et al. (2021), detailing the global carbon cycle. All values presented in Pg C yr^{-1}; yellow fluxes and pools (arrows and circles) represent historic conditions prior to the industrial revolution (1750 CE). Numbers in pink circles represent net changes in these stocks due to anthropogenic influence since 1750, while pink arrows represent average annual anthropogenic fluxes from 2010 – 2019. See full citations and original caption at URL: https://www.ipcc.ch/report/ar6/wg1/figures/chapter-5/figure-5-12.

Blue carbon; definition and productivity

Blue carbon as an ecosystem classification arose from the desire to highlight a particular ecosystem service found in coastal wetlands; the sequestration of greenhouse gasses (Laffoley, 2009; Lovelock & Duarte, 2019; McLeod et al., 2011; Nelleman et al.,

2009). Pursuant to this socio-political goal, Lovelock and Duarte (2019) established the following management-oriented criteria for the classification of coastal ecosystems as blue carbon systems (BCS): significant potential for greenhouse gas (GHG) capture or emission, long-term storage potential for sequestered GHG, presence of negative anthropogenic disturbance, feasibility of management for GHG reduction goals, lack of deleterious social or environmental effects resulting from interventions, aligning with other policies for climate change mitigation. While this definition scheme is demonstrably useful in communicating with broad audiences (evidenced by its broad adoption since inception in 2009), it was never going to last long in the quantitative world of the scientific community. A more biophysical definition has been suggested, defining BCS as "ecosystems that are influenced by marine waters that fix carbon dioxide and that store and accumulate it as organic carbon. They are bounded by the highest levels of tidal inundation at the terrestrial edge and by the limits of the photic zone in the marine edge" (Adame et al., 2024). Despite the increasingly explicit theoretical definition of BCS, the precise mapping at scales relevant to the management and protection thereof has not yet been accomplished (Adame et al., 2024). A large portion of BCS, "vegetated coastal habitats" (salt marshes, mangroves, seagrasses, and macroalgae) has been estimated to cover 2.3 - 7.0 million km^2 (0.2% of ocean surface, or < 3% of terrestrial forest extent); although this definition excludes tidal forests and includes macroalgal beds, thus failing to account for the full extent proposed by Adame et al. (2024), it nonetheless provides the best available estimate of the global extent of BCS and provides a useful if imperfect approximation (Duarte et al., 2013). Innumerable similar attempts have been made to

map or otherwise quantify the spatial extent of component BCS in different regions (Brophy, 2019; Duarte et al., 2013; Feagin et al., 2020; Kauffman et al., 2020; Kelleway et al., 2021; Krauss et al., 2018), but they universally suffer from inconsistent BCS definitions, and none include the entire BCS range from the landward tidal extent (*i.e.*, UEFW) to the marine photic boundary.

Blue carbon systems (BCS) have been found to be some of the most carbon-dense in the world (Adame et al., 2024; Donato et al., 2011) owing to their high rates of productivity (Kauffman et al., 2020) and low rates of C export through respiration or migration (Krauss et al., 2018; Noe et al., 2016; Spivak et al., 2019). BCS generally exhibit high C storage per unit area compared to other ecosystems (Table 1.1), with high stocks in both live vegetation and soils (Kauffman et al., 2020; Krauss et al., 2018), although the global reporting of total C storage in these systems is still suffering from a lack of data, especially of soil C contents (Kauffman et al., 2020). Despite their relatively small spatial extent, the total biomass of BCS is roughly equivalent to that of the terrestrial systems which dominate the earth's surface (Adame et al., 2024; Irving et al., 2011; Laffoley & Grimsditch, 2009). Carbon allocation patterns vary across the hydrogeomorphic gradients within BCS (Noe et al., 2016), with more C stored aboveground in freshwater tidal sites and more belowground C storage in relatively saline conditions (Donato et al., 2011; Krauss et al., 2018). Driving these C storage values are high primary productivity rates (GPP = 4.32 ± 2.45 gC m^{-2} day^{-1}, Feagin et al., 2020), extensive belowground productivity of local vegetation (Laffoley & Grimsditch, 2009), and soil biochemical conditions that inhibit bacterial respiration (Adame et al., 2024; Noe

et al., 2016; Spivak et al., 2019). These conditions are subject to high spatiotemporal variability due to the elevational, salinity, and tidal gradients along which BCS are found, and the quantification of this uncertainty is an ongoing area of investigation (Noe et al., 2016; Spivak et al., 2019). The long-term (century to millennial scale) sequestration of C relevant to the mitigation of climate change is driven by year-over-year burial in chemically reduced soils; as highlighted in the original definition of BCS, these are among the most efficient C-burying ecosystems in the world (Table 1.2; Irving et al., 2011; Laffoley & Grimsditch, 2009; Spivak et al., 2019). Annual rates of C burial in BCS have been estimated to offset between 0.9% and 2.6% of global anthropogenic CO_2 emissions (Feagin et al., 2020), with C burial rates per unit area of approximately 10 times that of temperate forests and 50 times that of tropical forests (Laffoley & Grimsditch, 2009).

Table 1.1. Globally averaged C stock density for terrestrial benchmark and "blue carbon" ecosystems

	Ecosystem	C density (Mg ha^{-1})	Range	Source
Terrestrial	Boreal Forest [a]	29.2	20.6 - 45.2	Anderson-Teixeira et al. (2018)
	Temperate Forest [a]	172.1	40.2 - 260.5	
	Tropical Forest [a]	370.4	274 - 488	
	Boreal Forest [f]	42	--	Huston & Wolverton (2009)
	Temperate Forest [f]	134	--	
	Tropical Forest [f]	194	--	
	Boreal Forest [b]	121.5	--	Penman et al. (2003)
	Temperate Forest [b]	179.4	111.0 - 323.0	
	Tropical Forest [b]	182.3	148.8 - 329.6	
	Wet [b, d]	231.6	168.2 - 364.9	
	Dry [b, d]	83.6	--	
Blue carbon	Saltmarshes [c]	450	100 - 800	Adame et al. (2024)
	Mangroves [c]	1043.5	79 - 2208	
	Seagrasses [c]	419.5	9 - 830	
	UEFW [c, e]	1026	358 - 1694	

Carbon densities reported across a variety of sources and methods. All density values represent mean estimates; ranges report observed min-max.

[a]: C density values compiled from the ForC database (Anderson-Teixeira et al., 2018)

[b]: C density values of forests > 20 years old, compiled from IPCC 2003 default values (Penman et al., 2003)

[c]: C density values as mean of ranges reported in Adame et al. (2024)

[d]: "Wet" / "Dry" delineation of tropical forests follows Penman (2003) terminology, based on 2003 IPCC guidelines

[e]: Termed "tidal wetlands" in Adame et al. (2024)

[f]: "current" (as of 2001) values only, from Huston and Wolverton (2009) Table 1

Table 1.2. Rates of C burial in soils of blue carbon and benchmark ecosystems

	Ecosystem		C burial (g C m^{-2} yr^{-1})	Source
Terrestrial	Boreal Forest [a]		0.8 - 2.2	(Laffoley & Grimsditch, 2009)
	Temperate Forest [a]		1.4 - 12.0	
	Tropical Forest [a]		2.3 - 2.5	
Blue carbon	Saltmarshes [a]		210	(Laffoley & Grimsditch, 2009)
	Mangroves [a]		139	
	Seagrasses [a]		83	
	UEFW		--	(Krauss et al., 2018, and refs therein)
		Freshwater Marshes [b]	80 - 435	
		Freshwater Forests [b]	7.0 - 336.6	

Values represent observed ranges or ecosystem mean estimates, as shown in the original source.
[a]: Laffoley and Grimsditch (2009) values calculated as long-term burial, accounting for century-scale remobilization
[b]: Krauss et al. (2018) values calculated from soil core observations; likely slightly biasing values higher compared to [a]

A Subset of a subset; zooming in on UEFW

The most widely recognized and studied components of BCS are saltmarshes, mangroves, and seagrass (Irving et al., 2011; McLeod et al., 2011; Spivak et al., 2019). However, the recent recognition of high C storage, GHG sequestration, and other defining BCS traits in tidal (sometimes supratidal) wetlands upstream of saltmarshes has led to the argument that these systems ought to be included in blue carbon inventories and management strategies (Adame et al., 2024; Kauffman et al., 2020; Kelleway et al., 2021; Krauss et al., 2018). Common language for these systems has not yet been established (G. Noe, pers. comm., 6-Mar-2024), with the terms “tidal freshwater forested wetlands” (TFFW), “supratidal forests,” “tidal wetlands,” “ghost forests,” and many more found in the literature, all describing ecologically and spatially diverse systems that nonetheless exhibit high C storage driven by marine influence (Figure 1.2), qualifying

them as “blue carbon.” Examples include oligohaline (< 0.5 psu) marshes found worldwide; *Taxodium/Nyssa* swamps found in the southeastern USA (W. H. Conner, Doyle, et al., 2007); *Casuarina/Melaleaca* swamps of Australia (Kelleway et al., 2021); *Picea* forests of the northwestern United States (Brophy, 2019; Kauffman et al., 2020), and many more (Adame et al., 2024). For the purposes of the current discussion, we use the term “upper estuarine forested wetlands” (UEFW) simply to keep things complicated. UEFW exhibit C densities (Table 1.1) and burial rates (Table 1.2) equivalent to or greater than averages found in other BCS, establishing these systems as similarly important in the understanding and management of the global C cycle. Despite the recent increase in attention to these systems, they remain a source of uncertainty (Krauss et al., 2018). The inclusion of UEFW to the BCS category has contributed to some of the confusion in global mapping described above, but certain subsets of UEFW have been delineated; for example, UEFW within the USA cover > 40,000 km^2 in South Carolina and > 23,000km^2 in Georgia (Field et al., 1991), but a mere 12.7 km^2 on the Oregon coast (Brophy, 2019). C cycle dynamics in UEFW are poorly understood on a global scale (Krauss et al., 2018), despite regional efforts to expand our understanding (*e.g.*, Kauffman et al., 2020; Kelleway et al., 2021; Krauss et al., 2018). The understanding of UEFW role in sedimentation and nutrient retention dynamics is less understood than that of other tidal wetlands but are known to have changed under both geologic-scale and anthropogenic changes to river sediment loads (Noe et al., 2016).

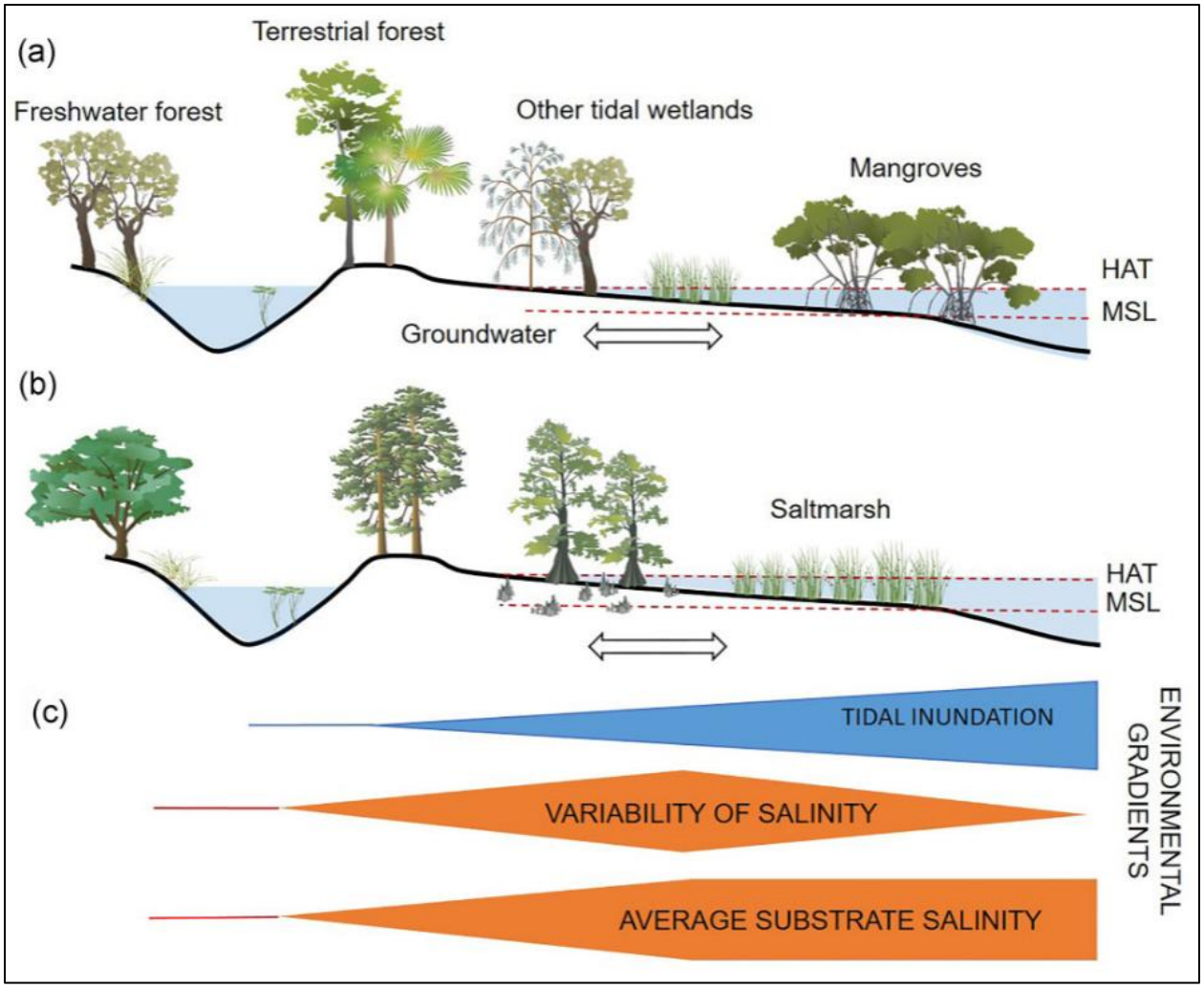

Figure 1.2. Reproduction of Figure 1 as originally published by Adame et al. (2024), depicting archetypal UEFW using (a) Australian *Casuarina* or *Melaleuca* forests or (b) cypress forests of the southeastern United States and the environmental and elevational distributions (c) along which these "other wetlands" are found. HAT: highest astronomical tide. MSL: mean sea level. URL: https://academic.oup.com/view-large/figure/444118846/biae007fig1.jpg

1.3 Understanding sap flow; the breath of the earth

Terrestrial transpiration, estimated at approximately 45,000 km^3, returns roughly 40% of all land precipitation back to the atmosphere (Oki & Kanae, 2006; Poyatos et al., 2021) and makes up about 70% of all land evapotranspiration (Flo et al., 2019). This is perhaps why the longstanding conceptualization of the movement of water through the terrestrial biosphere, the "soil-plant-atmosphere continuum" (SPAC), includes vegetation as an equal partner between the earth and the atmosphere (Goldsmith, 2013; Philip, 1966). Understanding the role of plants in the movement of water is therefore critical in the effort to manage watersheds at all scales (Chu et al., 2009; Dix & Aubrey, 2021b), especially in the context of predicted climatic changes (Allen et al., 2015). Sap flow measurements provide an important tool in the investigation of this step in the global hydrologic cycle at the individual plant level that cannot be obtained by ecosystem-wide water use estimators such as micrometeorological observations or modelling by surface energy or catchment water balancing (Maltese et al., 2018; Poyatos et al., 2016). These are valuable in both cross-validating other water use estimation methods (Peters et al., 2018) and parsing components of total evapotranspiration (Maltese et al., 2018; Oishi et al., 2008). Beyond the hydrologic cycle, sap flow methods can assess questions relating to plant physiology (Ewers & Oren, 2000), environmental response (Chu et al., 2009), stress adaptation (Oren et al., 1999), and other topics (Lu et al., 2004).

Gadgets and gizmos a 'plenty; a treasure trove of sap flow methods

Thermometric sap flow methods (TSM) have been broadly preferred over gas-exchange or isotopic tracking methods of tree-level transpiration monitoring (Flo et al., 2019) since the early 1980s due to their reliability, relatively high precision, and minimal destructive impact (Poyatos et al., 2016). Within this category is a cornucopia of individual methods which are not referred to uniformly across the body of scientific literature on the subject. However, Flo et al. (2019) provide a useful standardization framework by establishing four "families" within TSM; namely dissipation, pulse, field, and balance (Figure 1.3), as well as discussing their conceptual strengths and weaknesses and suitability for various applications (Table 1.3). The "balance" family (Figure 1.3 b), measuring the energy balance across a heated wood section, is the only direct measurement of the rate of sap flow in isolation (*i.e.*, g hr^{-1}), useful for whole-plant transpiration measurements; the other families (Figure 1.3 a) measure flux density in a given unit of sapwood area (*i.e.*, cm^3 cm^{-2} hr^{-1}), which can better discern spatial variability in the flow of water through a stem (Flo et al., 2019; Vandegehuchte & Steppe, 2013). Methods in the "pulse" and "field" families are capable of observing bi-directional flow (Goldsmith, 2013), which is often of interest in assessments of nocturnal sap redistribution (Green et al., 2009; Steppe et al., 2010). Of the flux density families, the "dissipation" family (specifically thermal dissipation methods (TDM), *e.g.*, Granier, 1987) is the most widely used by far (Poyatos et al., 2016) due to its relatively low cost and ease of use, despite a large body of work (Flo et al., 2019; Peters et al., 2018; Steppe et al., 2010) finding that the TDM underestimates total sap flow by 40% on average

(Poyatos et al., 2021). The TDM measures the removal of heat energy from a heated probe compared to a reference thermocouple, using established equations to convert the difference in temperature to rates of sap flux at the measured sapwood depth (Granier, 1987; Lu et al., 2004). All families of TSM have been shown to produce effective and applicable estimates of sap flow rates for given applications (Flo et al., 2019; Schlesinger & Jasechko, 2014), although researchers must evaluate the most appropriate methodology for a given research question (Table 1.3).

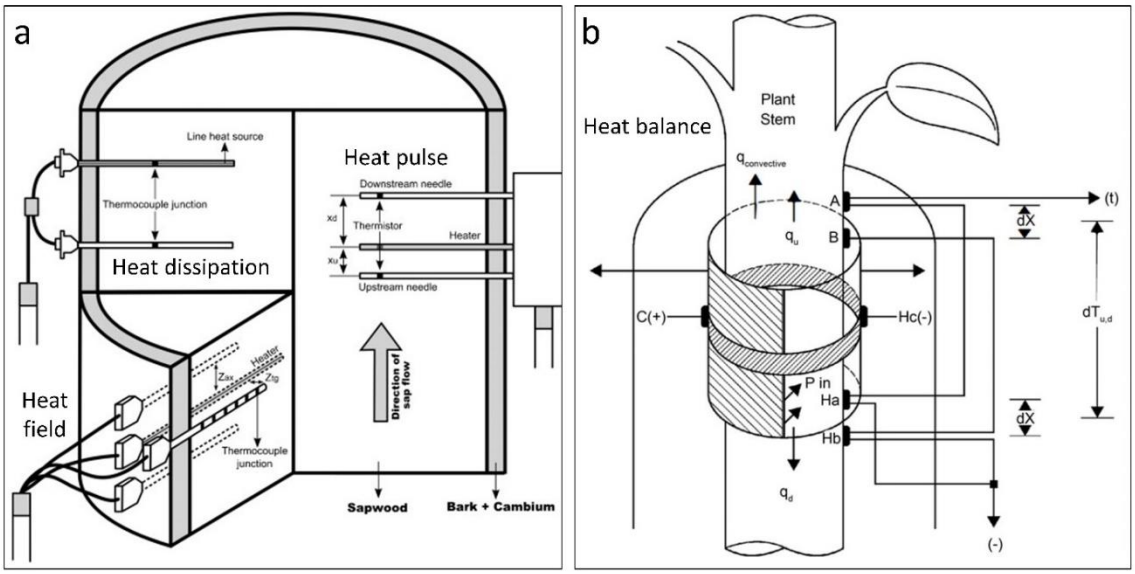

Figure 1.3. Reproductions of (a) Steppe et al. (2010) Figure 1 (modified), and (b) Lascano et al. (2016) Figure 1 (unmodified), depicting archetypal methods from each of the TSM families. Methods depicted in (a) include; thermal dissipation (*e.g.*, Granier, 1987) in the top left, heat field deformation (*e.g.*, Nadezhdina et al., 1998) in the bottom left, and compensation heat pulse heat pulse (*e.g.*, Steppe et al., 2010) on the right. The heat balance family in (b) is represented by the stem heat balance method adapted from its original patent (Van Bavel & Van Bavel, 1993). URL (Figure 1a): https://ars.els-cdn.com/content/image/1-s2.0-S0168192310001000-gr1.jpg. URL (Figure 1b): https://www.scirp.org/journal/paperinformation?paperid=70680#f1.

Table 1.3. Suitable applications and error sources for a variety of thermometric sapflow methods.

	Potential source of measure error									*Effectiveness in measuring*					
Method	***Wounding***	***Radial velocity profile***	***Wood properties***	***Natural thermal gradients***	***Sensor installation***	***Sensor design***	***Baselining***	***Power input***	***Pulse length***	***Reverse flows***	***Low flows****	***High flows****	***Absolute flows***	***Relative flows***	***Small stems***
CHP	x	x	x	x	x				x						
T-max	x	x	x		x		x								
HR	x	x	x		x										
HFD	x	x		x	x	x	x	x							
SHB				x			x	x							
TD	x	x	x	x		x	x	x							
TTD	x	x	x	x		x	x	x							

An unmodified reproduction of Flo et al. (2019) Table 4, depicting the effectiveness of various TSM applications. Methods include the; compensation heat pulse (CHP), T-max, and Heat Ratio (HR) methods from the "pulse" family; heat field deformation (HFD) from the "field" family; stem heat balance from the "balance" family; and thermal dissipation (TD) and transient thermal dissipation (TTD) from the "dissipation" family. On the left side of the table, crosses represent that a given method is sensitive to an error source, which is updated from Vandegehuchte and Steppe (2013). On the right side of the table, darker cells indicate that a given method is more appropriate for a given application, while white cells represent that the method is unsuitable. URL: https://www.sciencedirect.com/science/article/pii/S0168192319301248#tbl0020
*: low/high values for SFD methods are $< 5 / > 80$ cm^3 cm^{-2} hr^{-1}, respectively, and $< 260 / > 3900$ cm^3 hr^{-1}, respectively, for SF methods (only SHB)

Whosits and whatsits galore; all the things we're still learning

Methodological limitations to TSM (*i.e.*, factors intrinsic to the technology or the application thereof) have been the source of discussion in the literature since its inception (Čermák et al., 1984; Dixon, 1914; Granier, 1987), and have shown no signs of slowing down (Flo et al., 2019; Peters et al., 2018; Poyatos et al., 2021; Vandegehuchte & Steppe, 2013). One such methodological limitation is the inevitable wounding effect caused by the insertion of the probes themselves (Wiedemann et al., 2016), resulting in the compartmentalization of wounded tissue over time (Dujesiefken et al., 1999) and under-estimations (sometimes "dampening") of flow densities (Peters et al., 2018; Steppe et al., 2010). These wound effects have been estimated to have the largest contributions to systematic TDM uncertainty (Steppe et al., 2010; Wiedemann et al., 2016), and to reach their full impact at around 2 weeks after installation in oak and beech trees, although uncertainties remain regarding how wounds might develop in different species and across environmental conditions (Wiedemann et al., 2016). The availability of corrective equations for the wounding effect (*e.g.*, Green et al., 2009; Wiedemann et al., 2016) or non-invasive probes (*e.g.*, Clearwater et al., 2009) varies across the TSM families, but have not been available for the widely used TDM until very recently, and their application is yet to be routinely adopted (Flo et al., 2019; Peters et al., 2018; Wiedemann et al., 2016). The dissipation, field, and pulse families, sometimes referred to collectively as "sap flux density methods," are all dependent to varying degrees on the establishment of accurate empirical relationships between temperature and sap flux density (Clearwater et al., 1999; Flo et al., 2019; Lu et al., 2004). The calibration of these empirical

relationships at both the site- and species-level is also yet to be routinely adopted, despite having been recommended extensively since at least 2004 (Dix & Aubrey, 2021b; Lu et al., 2004) to resolve the greatly divergent accuracy of sap-flow-derived transpiration rates across the field (Dix & Aubrey, 2021a; Krauss et al., 2015; Peters et al., 2018). The misalignment of sensor geometry (Ren et al., 2017), potential for poor wood-to-sensor contact (Clearwater et al., 1999), variable sensor construction (Lu et al., 2004), and even the processing of raw data (c.f. Oishi et al., 2016; Peters et al., 2021) are all additional sources of variability in the sap flow literature which similarly have varying availability of mathematical or methodological corrections across families (Table 1.3), but remain under-applied in the breadth of the literature (Flo et al., 2019; Peters et al., 2018).

Zero-flow conditions are fundamental to the calculation of sap flow values in most TSM (Table 1.3, column "baselining"), historically assumed to occur during the early morning before sunrise (Granier, 1987). However, non-negligible nighttime sap flow is frequently caused by a variety of factors (Lu et al., 2004), presenting a hurdle for the accurate estimation of sap flow values (Oishi et al., 2008, 2016). The establishment of a dynamic baseline between occurrences of zero-flow conditions accounts for the fact that these may not occur every night and prevents the resultant underestimation of sap flow values (Lu et al., 2004). The identification of these zero-flow conditions is non-trivial and has only recently been semi-automated by several divergent software solutions (Oishi et al., 2016; Peters et al., 2021; Ward et al., 2017). Four distinct methods for determining zero-flow conditions were collated and compared by Peters et al. (2018); a simple daily predawn value from between 00:00 and 08:00, a moving window of the

predawn value in an 11-day window, double regression described in Lu et al. (2004), and the environmentally dependent method developed in recent software releases (Oishi et al., 2016; Peters et al., 2021; Ward et al., 2017). The environmentally dependent and double regression methods of zero-flow determination showed the most promise and were recommended for future applications (Peters et al., 2018). The same review found that 42% of publications using the TDM since 2010 fail to report the use of any zero-flow procedure (Peters et al., 2018), agreeing with other authors that the determination of zero-flow conditions is a significant error source in TSM applications (Flo et al., 2019).

Beyond the methodological errors inherent to sap flow monitoring, there are a variety of environmental and physiological sources of error that contribute to the chronically high variability in the estimates of plant water use via TSM (Flo et al., 2019; Poyatos et al., 2021; Steppe et al., 2010). While the theoretical model of tree response to environmental factors is well-established (Ewers & Oren, 2000), the specific contributions of each component of the soil-plant-atmosphere pathway (Oren et al., 2001) have yet to be fully quantified, including many open questions regarding plant-level variation across environmental gradients (Poyatos et al., 2016). Environmental sources of error include the susceptibility of TSM to short-timescale variability in flow due to high wind (Chu et al., 2009), artificially high morning flow estimates due to natural temperature gradients (sometimes “natural thermal gradients” or NTG; see Table 1.3) caused by the flow of cool water into relatively warm stems (Reyes-Acosta et al., 2012), and the suppression of overall daily sap flow caused by short precipitation events or cloud cover that are difficult to screen via weather monitoring (Lu et al., 2004). The

effect of tree physiological traits on measured sap flow values and the extrapolation thereof are also not fully understood (Kotowska et al., 2021), partially accounting for the highly divergent water use estimates produced between various methodologies (Fan et al., 2018; Steppe et al., 2010). Spatial variation in sap flux density throughout the stem can be driven in part by hydraulic characteristics such as inter-annual ring porosity and vascular anatomy (*e.g.*, vessel diameter, wood density, etc.; Berdanier et al., 2016; Kotowska et al., 2021), sometimes resulting in radial or azimuthal attenuation curves with sufficient magnitude to impact whole-plant water use estimations if unaccounted for (Berdanier et al., 2016; Fan et al., 2018; Flo et al., 2019; Oren et al., 1999; Peters et al., 2018). A recent review found that only ~ 34% of TDM studies accounted for azimuthal variation, and only ~ 43% accounted for radial variation (Poyatos et al., 2021), and those studies which do make the attempt frequently lack the sample size to reach adequate statistical power (Krauss et al., 2015). Tree size class can also reduce sap flux density, with Oren et al. (1999) finding that trees in the lower third of the diameter distribution had only 70% the flux density of those in the other two-thirds of the distribution. The systematic impact of plant water capacitance and recharge on TSM measurements is also not fully understood, but it is increasingly accepted that flows related to water uptake rather than transpiration are common under a variety of environmental conditions (Krauss et al., 2015), as demonstrated by the continuation of stem sap flow after flow in branches has ceased (Ewers & Oren, 2000). The storage of water in vascular tissue generates lag in the response of sap flow to driving environmental variables (Ewers & Oren, 2000; Oren et al., 1999). These environmental and physiological errors are not always effectively

integrated in basic scaling approaches where stand sapwood area is assumed to conduct equally (Berdanier et al., 2016).

Scaling from sapwood to stand-level estimates

Intrinsic to TSM is a mismatch between the scale of observation (sapwood cross-sectional area) and the most commonly interesting outputs; the estimation of stand- or landscape-scale transpiration (Ward et al., 2015). Scaling from sample to ecosystem carries the implicit assumption that any systemic biases are represented (Berdanier et al., 2016; Oren et al., 1999); any un-accounted biases (such as the previously discussed sources of error) are inevitably propagated across scales from sensor to tree and beyond (Oishi et al., 2016; Oren et al., 1999; Poyatos et al., 2016). The estimation of stand-level sapflow requires, at minimum, quantification of variation by depth, azimuth, size class, nutrient status, and light competition status (Ewers & Oren, 2000; Oren et al., 1999); the routine failure to assess these values (Fan et al., 2018; Peters et al., 2018; Poyatos et al., 2021) limits the strength of TSM data in water use estimation. For example, a recent review found that of 122 papers which used sap flux measurements to scale to stand or tree level water use, 58% failed to account for radial variation entirely (Berdanier et al., 2016). A systematic quantification of the variability induced by all the discussed error sources has not been undertaken (Merlin et al., 2020; Peters et al., 2018). This propagation is mitigated somewhat in systems which have been subject to a greater survey effort; temperate forests, representing 80% of the data in a recent database collation, are likely the most well-understood ecosystems in terms of sap-flux-based

transpiration estimates (Poyatos et al., 2021). On the other end of the spectrum, tropical and boreal forests, as well as forested wetlands are all chronically under-studied ecosystems that are subject to higher levels of uncertainty (Krauss et al., 2015; Poyatos et al., 2021).

TSM applications

Despite these many sources of uncertainty in the field of sap flow measurement, TSM have provided an array of applicable insights that broadly agree with external validation (Flo et al., 2019; Schlesinger & Jasechko, 2014). Sap flow measurements have been extensively applied to investigations of plant and ecosystem physiology, including drought adaptation (Poyatos et al., 2016), the role of stomata in the regulation of transpiration across environments (Ewers & Oren, 2000), whole-tree physiological response to irrigation and fertilization treatments (Lu et al., 2004), and water use adaptation across life history adaptations (*i.e.*, successional stage or shade tolerance, Oishi et al., 2008). These findings have been informing agricultural and restoration management strategies for several decades (Dix & Aubrey, 2021b). Krauss et al. (2015) present a modelling method which either incorporates or resists many error sources in the estimation of stand water use of forested wetlands. The recent development of a whole-tree water use model which incorporates both wood type and radial attenuation provides a more broadly applicable tool, although still lacking the incorporation of azimuthal variation (Berdanier et al., 2016). The emergence of a global database containing standardized sap flow measurements (Poyatos et al., 2016) also presents new

opportunities to assess and control the systematic sources of error discussed herein, as well as to apply TSM findings across broader spatial and taxonomic scales.

1.4 Conclusion

This review of UEFW C dynamics and sap flow estimation has identified both the utility and shortcomings of the respective fields. The assessment of C stocks in UEFW is a recent development but has demonstrated promising early values that place these systems among the most high-priority ecosystems to provide the necessary C storage to assist in the mitigation of anthropogenic climate change. A wide variety of questions remain to be addressed by future UEFW C storage studies, including the resolution of fine-scale spatiotemporal variability in conditions that promote C burial and primary production. The use of sap flow methods to investigate ecophysiological questions is significantly older, having informed both water use budgets and our understanding of tree physiology for decades, but is still subject to continuously updating methods. Recent developments in both the global integration (*i.e.*, the SAPFLUXNET initiative) and modelling of sap flow values and their methods of acquisition have increased the applicability of the technology, while the establishment of species- and site-specific empirical calibrations represents a massive body of work that awaits new investigation. The following chapters represent the authors' attempts to contribute to these diverse fields.

CHAPTER TWO

ABOVEGROUND CARBON STOCKS ACROSS A HYDROLOGICAL GRADIENT: GHOST FORESTS TO NON-TIDAL FRESHWATER FORESTED WETLANDS

2.1 Introduction

Blue carbon ecosystems such as seagrass beds, salt marshes, and mangroves have rates of carbon (C) burial (138 – 218 g C m^2 yr^{-1}) which greatly outpace that of terrestrial forests (4 – 5 g C m^2 yr^{-1}) (McLeod et al., 2011), distinguishing these habitats as being of critical importance in understanding the global C cycle and driving extensive scientific investigation on their potential to reduce atmospheric C concentrations (Bridgham et al., 2006; Chmura et al., 2003; Kauffman et al., 2020; Krauss et al., 2018; McLeod et al., 2011; Pendleton et al., 2012; Smith et al., 2019). Only recently included in blue C inventories, Upper Estuarine Forested Wetlands (UEFW), also referred to as tidal freshwater forested wetlands (TFFW), are found spanning the estuarine gradient between traditional freshwater nontidal wetlands and lower elevation blue C ecosystems (Adame et al., 2024; Noe et al., 2016). This estuarine gradient is composed of contributory hydrogeomorphic transitions in elevation, salinity, and tidal influence (Adame et al., 2024) which are typical of the riverine-estuarine boundary. The position of UEFW along this complex interface of terrestrial and maritime environments enables them to play critical roles in local ecology (Conner et al., 2007a; Field et al., 1991; Kauffman et al., 2020; Pendleton et al., 2012) and coastal biogeochemistry (*i.e.*, sediment and nutrient retention; Noe et al., 2016), while exhibiting large (Jia et al., 2019) but often imprecisely

quantified (Houghton et al., 2009) aboveground standing C stocks and burial rates (Field et al., 1991; McLeod et al., 2011; Santoro et al., 2021). These diverse UEFW are subjected to a complex set of environmental drivers including the presence of freshwater tidal flushing at their landward distributional limit and salinity pulsing more seaward (Conner et al., 2007a; Hackney & Avery, 2015; Krauss et al., 2009), creating a rarely described series of drivers to the ecology of any functionally freshwater ecosystem. Because UEFW are not identified by a specific vegetation type, they are difficult to map, often seen as simply transitional, and often overlooked (Conner et al., 2007b). However, UEFW occupy thousands of hectares in the southeastern US alone (Doyle et al., 2007), and are present in many other countries (*e.g.*, Duberstein et al., 2014; Kelleway et al., 2021).

To quantify C stocks in UEFW along two Southeastern US rivers, our study sites span the estuarine gradient, including nontidal freshwater floodplain swamps just bordering the estuarine boundary, past the head-of-tide into TFFW and down to the lowest extent of forested wetlands. There, salinity and hydroperiod have transitioned the tidal forests into oligohaline marshes (Conner et al., 2007a; Davis et al., 1981; Ensign et al., 2014; Hackney & Avery, 2015). This gradient represents a space-for-time transect design, allowing inference of potential future migration of lower estuary wetland systems to more upstream locations with future sea level rise (SLR) (Conner et al., 2007a; Craft et al., 2009; Ensign et al., 2014; Jia et al., 2019). Relative SLR on the lower Atlantic coastal plain averaged 3.5 mm yr^{-1} since the 1920s (NOAA gauge 8665530, Charleston, South Carolina), but regional accelerations to as high as 9.8 mm yr^{-1} have been reported in the

Southeastern US (Parkinson & Wdowinski, 2023). Modelling efforts based on similar SLR rates predict an increase of 14% in area occupied by nontidal swamps and a decrease of 24% in area occupied by TFFWs in the southeastern US over the next 100 years (Craft et al., 2009). Historical data for all blue carbon ecosystems indicate annual decreases of 0.7 - 7% due primarily to land-use changes (McLeod et al., 2011). Thus, regional rates of loss reported by Craft et al. (2009) strongly exceed rates from other blue C ecosystems due primarily to damming, diking, ditching, and development.

Assessments of C allocation across UEFW are exceedingly rare (Barendregt et al., 2009; Conner et al., 2007b; Kauffman et al., 2020; Krauss et al., 2018; Noe et al., 2016; Pendleton et al., 2012), except for recent work in blue C systems such as tidal marshes and seagrass beds (McLeod et al., 2011; Pendleton et al., 2012). While the majority of C is stored belowground in blue carbon ecosystems (Donato et al., 2011), aboveground biomass dynamics are more uncertain in time owing to episodic events and stress-imposed structural shifts, but as noted by the Global Climate Observing System, aboveground biomass is a critically important variable in linking C dynamics to climate modelling (Santoro et al., 2021). The temporal dynamics of aboveground C have been sorted in many other blue carbon ecosystems (*e.g.*, Kwan et al., 2022; Safwan Azman et al., 2023) but not for UEFW. Here, we investigate three new aspects of aboveground C dynamics for UEFW. First, aboveground C biomass changed between + 15.1% to - 74.4% over a 7-year period while dead standing biomass increased by as much as 142% for UEFWs along the Waccamaw and Savannah rivers (Krauss et al., 2018), prompting concern for how rapidly aboveground C changes may occur along these and other

transitional UEFW environments both naturally and in model simulations (*e.g.*, Wang et al., 2022). We extend this record for another 8 - 10 years to focus specifically on this metric of change. Second, we augment the landscape context for aboveground C storage by adding sites farther inland where we hypothesize that future sea-level rise driven change is imminent. Third, we add to the salinity-stress literature, which often focuses on seedlings (Duberstein et al., 2020), by adding information on how salinity affects coastal C balance at the ecosystem scale.

2.2 Methods

Location

UEFW C standing stocks were assessed on a series of 5 study sites along estuarine gradients of both the Savannah River and the Winyah Bay system, comprised of sites on the Waccamaw, Pee Dee, and Sampit rivers. Three UEFW research areas were established in 2004, with hydrologic conditions including semidiurnal tidal inundation and ranging from oligohaline to entirely freshwater (Krauss et al., 2009). In 2020 two additional study areas were established on each river/estuary system to include an area near the upper extent of tidal influence that has a seasonal belowground tidal signature ("head of tide"), and to an area that experiences no tidal flooding throughout the year ("nontidal"), but which still experiences tidal influence within the channel of the adjacent river (Figure 2.1). Each study site contained two 20 x 25 m plots which included 2 water monitoring wells and five 0.25 m^2 litter traps. Long-term soil porewater salinity conditions at the 3 estuarine sites have been previously described (Krauss et al., 2018),

ranging from exceeding 4.0 ppt at heavily salt impacted UEFW (“lower” sites), to generally 1.2 – 1.4 ppt at moderately salt impacted UEFW (“middle” sites), and very low or nonexistent salinity (~0.1 ppt) at continuously fresh UEFW (“upper” sites). Data for this study was collected from the summer of 2020 to the spring of 2022.

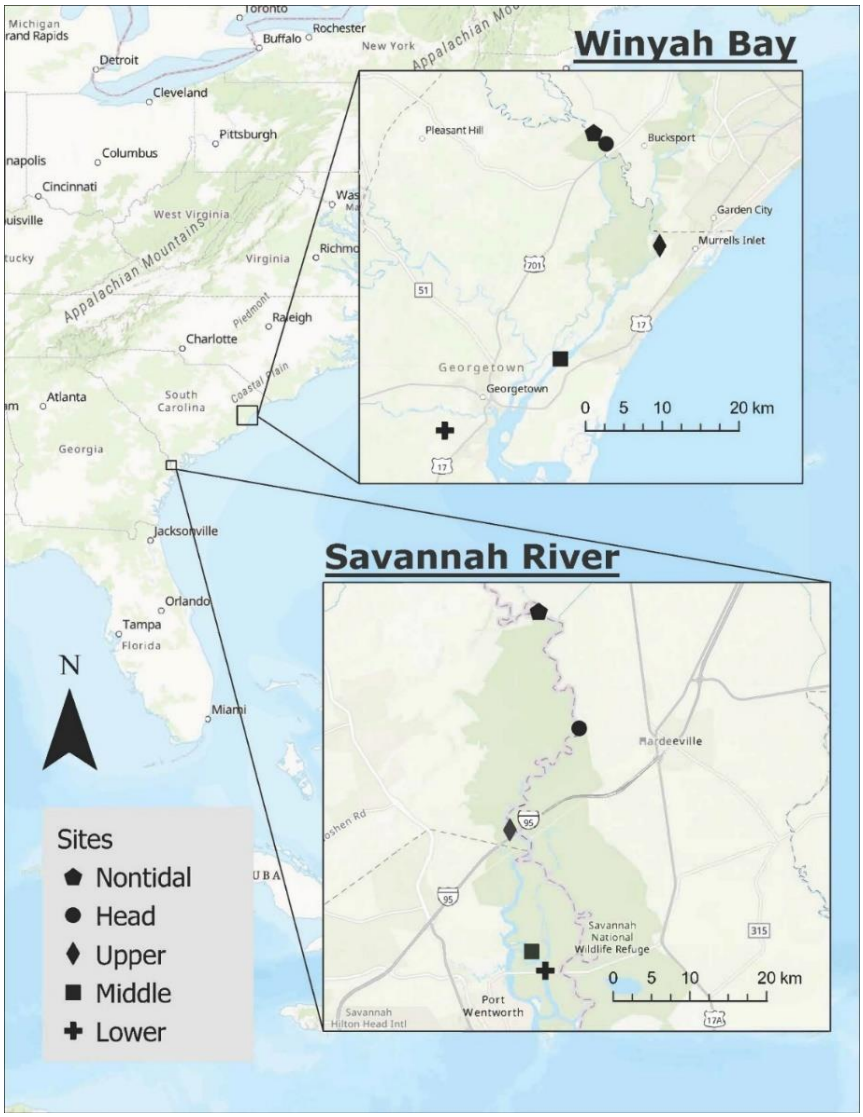

Figure 2.1. Site locations within the southeastern Atlantic coast of the United States including the Savannah River and Winyah Bay systems in Georgia and South Carolina, respectively.

Data collection & calculations

Porewater salinity was measured monthly throughout the data collection period of this project (2020 – 2022) using a handheld water quality instrument (model Pro30, YSI Inc., Yellow Springs, OH, United States). Water level data were collected using a continuously deployed non-vented pressure transducer (models LT/LTC 3001 and Levelogger Edge M10, Solinst Canada Ltd, Georgetown, ON, Canada) which was post-processed using atmospheric pressure data collected simultaneously from on-site barometric pressure sensors (model LT 3001 Barologger Edge M1.5, Solinst Canada Ltd., Georgetown, ON, Canada). Four salinity monitoring wells were installed near the corners of the plots. Monitoring wells were constructed from 3.2 cm diameter slotted schedule 40 PVC with the bottom end of the well permanently capped. These wells were inserted to a depth of ~ 91 cm. The final 60 cm of the well was slotted and wrapped in a fiberglass screen to help reduce the infiltration of sediments. The height of the well above the ground varied to allow researchers access during flooding events.

Carbon stocks of trees, snags, shrubs, and saplings were estimated using the Forest Inventory Analysis Component Ratio Method (FIA-CRM) as established by the US Forest Service (USDA Forest Service, 2019). Many authors in the allometric modelling field have argued that uncertainty related to the selection of allometric equations (*i.e.*, species-specific vs generic models) contributes significantly to modelling error (Chaturvedi & Raghubanshi, 2013; Chave et al., 2014; Fonseca et al., 2012; Vorster et al., 2020). It is likely that trees in transitional environments such as salinity-impacted swamps exist in conditions that deviate from established allometry, thus contributing a

potential source of error (Houghton et al., 2009; Vorster et al., 2020). Nonetheless, the need for standardization is clear in the context of nationwide datasets to which we wish our UEFW observations to be compatible (Clough et al., 2016; Houghton et al., 2009). For this reason, we chose to use the FIA-CRM rather than generic (*i.e.*, Jenkins et al., 2003) or simple linear (*i.e.*, Clough et al., 2016) methods of allometry.

To assess total aboveground C stocks, we measured standing live trees, live shrubs, live saplings, litterfall, standing dead trees, coarse woody debris, and fine woody debris. Woody stem measurement in our study follows the methods laid out in the FIA field guide 9.0 (USDA Forest Service, 2019). Stems within our plots were sorted into trees, saplings, shrubs, and snags during analysis, but during data collection were treated uniformly. All live woody stems greater than 2.5 cm diameter at breast height (DBH, 1.3 m aboveground) and taller than 1.3 m were DBH-measured. Heights of each tree were measured using a digital hypsometer (models Vertex IV and Transponder T3, Haglof Inc., Långsele, Sweden). Tree diameters were measured using standard D-tapes when stems were larger than 2.5 cm, while analog calipers were used for smaller stems. Levels of decay on dead standing trees were estimated following Domke et al. (2011). Percent cull for snags was estimated based on decay class; classes 1 & 2 were 0%, class 3 was 20%, class 4 was 50%, and class 5 was 75%. Dead trees (snags) were not included in the survey if their DBH was < 10.0 cm. Due to the frequently flooded nature of our plots, we placed less subjective weight on a snag's basal decay than is indicated in the table, under the assumption that rot at the base of a snag was accelerated by site conditions and did not accurately reflect the decay state of the entire bole. Biomass (kg) of these various

woody stems was calculated using the Component Ratio Method (CRM) as established by Woodall et al. (2011) and adopted by the US Forest Inventory Analysis (USDA Forest Service, 2019) program. In this method, tree height, diameter, and cull are figured into region- and species-specific equations to calculate biomass of stems including bark and stump, but not foliage. All woody specimens were sorted by stem diameter; trees were defined as any stem ≥ 10.0 cm DBH, saplings were defined as any stem between 2.5 cm and 10 cm DBH, and shrubs were defined as any stem which was < 2.5 cm DBH but ≥ 2.5 cm at 0.3 m above the root collar. Sapling biomass was calculated according to Heath et al. (2009), which adapts the CRM to smaller stem sizes seen in this size class. Shrub biomass was calculated using a generalized hardwood model (Day & Monk, 1974), which permits calculation of still-smaller stems than the Heath method. Snag biomass was calculated according to Domke et al. (2011). All live wood biomass was assumed to be 50% C by dry weight.

Foliar biomass (MgC ha^{-1}) was measured for each site using ten 0.25 m^2 litter traps distributed evenly throughout the area. Litter traps were approximately 1.2 m tall, and thus represent both overstory and understory litterfall. Samples were collected monthly between April 2021 and March 2022 and dried at 70° C for at least 3 days before weighing. Foliar mass was also assumed to be 50% C by dry weight, as established by previous work in the system (Krauss et al., 2018). Average monthly litter weights (g C m^{-2}) were then summed across the study duration to assess the total annual foliar production at a given site, which is treated as the plot's foliar standing stock in Mg C ha^{-1}.

Understory stocks were estimated following the methodology of Ensign et al. (2014). Herbaceous plants were sampled quarterly between Spring 2021 and Winter 2022 utilizing two 25 m transects perpendicular to the river channel, placed outside our existing forest inventory plots making them ~ 50 – 100 m apart. Five 0.25 m^2 plots were located pseudo-randomly along each transect. Species within the plot were identified, sorted into live and dead biomass, dried at 70° C for ≥ 5 days, and weighed. Herbaceous biomass for each site was calculated by averaging the ten samples per site for each season. The four seasonal herbaceous values were then summed to annualize herbaceous C standing stock. Herbaceous dry mass values were converted to C using established ratios (Krauss et al., 2018) of 38.35% C for live mass, and 36.25% C for necromass. Necromass and live mass were both included in herbaceous biomass inventory values.

Downed woody debris (DWD) was measured using the line-intercept technique originally presented by Van Wagner (1968). In each site, 20 m transects originating from the centers of the two subplots were established. We divided each subplot into quarters delineated by the cardinal directions as measured from the center point; a transect was placed within each quarter along a random heading. In this way, 4 transects per subplot were established in an attempt to overcome the high variability often observed in DWD data (Ricker et al., 2019). Along the full length of each transect, all debris with diameter > 7.5 cm was recorded for diameter and decay class. Decay class was separated into one of three categories: sound, intermediate, and rotten. Sound debris was fresh and possessed no detectable decay, while rotten wood was easily penetrated by measurement calipers (Krauss et al., 2005). For the first 4 m of the transect, fine woody debris with

diameters between 1 cm and 7.5 cm were tallied. Ultra-fine woody debris with diameters < 1 cm was tallied for the first 2 m of the transect as well. The total mass of DWD was calculated at line intercept where each debris fragment's volume in m^3 is calculated by the following formula:

$$v = \left[\pi^2 \left(\Sigma d_i^2\right)/8\, L\right] * \mathrm{k}$$

Where d_i is the diameter of a fragment in m, L is the sample line's length in m, and k is the per-ha conversion constant (Van Wagner, 1968). As our data for fine and ultra-fine debris were tallied based on size class, these counts were assumed to have the median value for their range. Fine woody debris was assumed to be 4.25 cm in diameter, and ultra-fine was assumed to be 0.5 cm in diameter.

2.3 Results

On the Savannah River, salinity ranged from 1.6 – 6.5 ppt (avg 3.4 ppt) on the most seaward site (lower), and from 0.2 – 1.3 ppt (avg 0.4 ppt) on the next site upriver (middle). Similarly, salinity values on the Winyah River ranged from 0.4 – 4.1 ppt (avg 1.6 ppt) on the "lower" site and 0.1 – 2.2 ppt (avg 0.5 ppt) on the "middle." Salinity values on the "upper," "head-of-tide," and "nontidal" sites on both rivers were consistently low, averaging below 0.2 ppt throughout the study duration. Inundation patterns varied across the estuarine gradient, driven by river flow rates and the low relief of the southeastern coastal plain. Sites towards the riverine boundary of the estuary (nontidal and head-of-tide) tended to be dominated by low-frequency, high-duration

flooding while sites on the seaward side of the estuarine gradient (upper, middle, and lower) were defined primarily by semidiurnal tidal cycles (Figure 2.2). Water levels at semidiurnally tidal sites (upper, middle, and lower) on the Savannah River showed a range from -0.5 – 0.5 m, while on the Winyah River they fluctuated from -1.5 – 1.1 m across the duration of the study. Nontidal and head-of-tide sites on the Savannah River ranged from -1.4 – 1.3 m, while on the Winyah River they ranged from -0.4 – 1.2 m. "Upper" sites on both rivers were just upstream of salinity intrusion, showing negligible porewater salinity values akin to the "nontidal" and "head-of-tide" sites, but still within the elevational range to be subject to semidiurnal tides akin to the "middle" and "lower" sites.

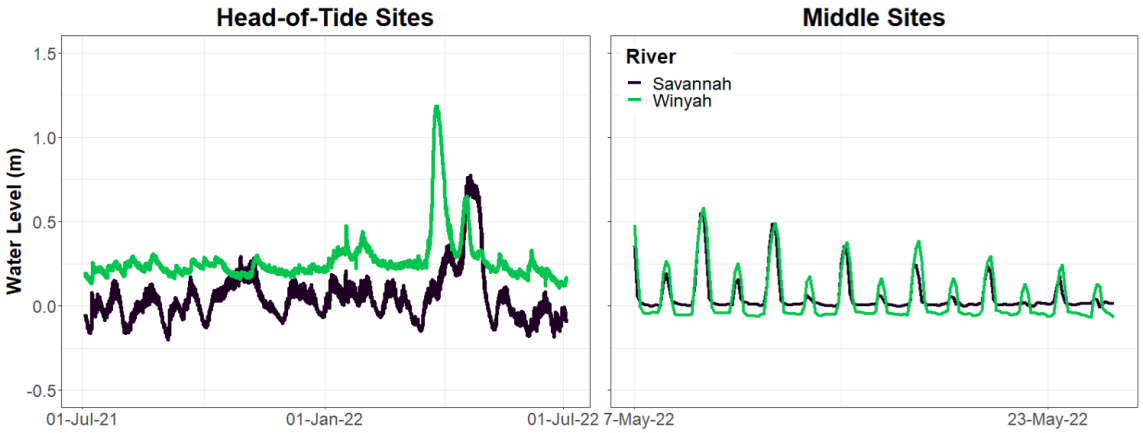

Figure 2.2. Water level patterns vary across the estuarine gradient of the systems, being characterized as either low-frequency, high-magnitude (left) or semidiurnal (right) flood patterns. Note that the two hydrographs show different temporal scales on the x-axes, but the same meter scale on the y-axes.

On the Savannah River, total aboveground C storage in vegetation ranged from 287.0 Mg C ha^{-1} to 28.1 Mg C ha^{-1}. On the Winyah system, total C values ranged from 221.6 Mg C ha^{-1} to 38.0 Mg C ha^{-1}. Both rivers showed markedly similar total C values across their UEFW gradient (Table 2.1). On both rivers, we observed the expected decrease in aboveground C corresponding with the increasing salinity of the lower-estuary plots (lower and middle sites, Figure 2.3). On all sites except for one (Savannah lower), trees dominated the total aboveground C makeup of our plots, accounting for an average of 88.2% of aboveground C. Savannah lower had near complete die-off of trees since its original establishment in 2005, and consequently trees accounted for only 9.5% of aboveground biomass there, with the majority of C being stored instead in standing snags (16.9 Mg C ha^{-1}, 60.1%).

Table 2.1. C stocks at study sites along the Winyah and Savannah rivers

	Winyah river					Savannah river				
	Nontidal	Head	Upper	Middle	Lower	Nontidal	Head	Upper	Middle	Lower
Total aboveground C	217.2	221.6	210.8	123.7	38.0	287.0	207.8	222.7	172.2	28.1
Live trees	197.0	192.0	200.0	111.9	23.9	254.1	189.1	208.0	164.0	2.7
Saplings	1.7	5.4	1.8	0.3	0.2	2.0	1.3	4.1	0.2	0.0
Shrubs	0.00	0.00	0.15	0.02	0.00	0.27	0.00	0.66	0.00	0.57
Foliage	3.16	2.48	3.49	2.39	0.43	2.92	2.51	2.51	1.55	--
Herbs	0.01	0.00	0.26	0.87	1.04	0.05	0.05	0.24	0.49	4.04
Snags	1.3	7.8	0.4	1.7	9.9	0.0	6.8	2.0	1.5	16.9
FWD	11.9	11.1	3.6	5.0	1.3	13.8	4.2	4.3	3.6	1.7
CWD	2.1	2.8	1.1	1.5	1.3	13.8	3.8	1.0	0.8	2.2
mean salinity (range)	0.2 (0.1 - 0.3)	0.2 (0.1 - 0.3)	0.1 (0.0 - 0.1)	0.5 (0.1 - 0.3)	1.6 (0.4 - 4.1)	0.1 (0.0 - 0.2)	0.2 (0.1 - 0.3)	0.1 (0.1 - 1.3)	0.4 (0.2 - 1.3)	3.4 (1.6 - 6.5)

Values represent average Megagrams of Carbon per hectare (Mg C ha^{-1}) of a given biomass pool in each of our sites. Two subplots per location were averaged. The Savannah Lower site did not have enough trees to warrant the placement of litter traps, and therefore does not have a foliage value.

Table 2.2. Tree species contributions to standing biomass stocks.

Winyah

Nontidal			Head			Upper			Middle			Lower		
Species	C (Mg ha^{-1})	%	Species	C (Mg ha^{-1})	%	Species	C (Mg ha^{-1})	%	Species	C (Mg ha^{-1})	%	Species	C (Mg ha^{-1})	%
w. tupelo	102.85	52.2%	water tupelo	115.59	60.21%	baldcypress	161.61	80.79%	baldcypress	109.13	97.52%	baldcypress	23.94	100.00%
baldcypress	93.25	47.35%	baldcypress	54.82	28.56%	red maple	21.03	10.52%	w. tupelo	1.53	1.37%			
water elm	0.74	0.37%	water elm	6.88	3.58%	s. tupelo	17.16	8.58%	s. tupelo	1.24	1.11%			
red maple	0.12	0.06%	laurel oak	4.64	2.42%	ash	0.18	0.09%						
			s. cottonwood	2.47	1.29%	laurel oak	0.03	0.02%						
			ash	2.43	1.26%	waxmyrtle	0.02	0.01%						
			white oak	1.70	0.88%									
			sweetgum	1.54	0.80%									
			red maple	1.24	0.64%									
			s. tupelo	0.51	0.27%									
			deciduous holly	0.15	0.08%									

Savannah

Nontidal			Head			Upper			Middle			Lower		
Species	C (Mg ha^{-1})	%	Species	C (Mg ha^{-1})	%	Species	C (Mg ha^{-1})	%	Species	C (Mg ha^{-1})	%	Species	C (Mg ha^{-1})	%
baldcypress	130.41	51.33%	baldcypress	91.59	48.44%	baldcypress	91.74	44.11%	baldcypress	162.65	99.17%	baldcypress	2.35	88.54%
w. tupelo	115.72	45.55%	water tupelo	83.13	43.97%	w. tupelo	63.26	30.42%	s. tupelo	1.36	0.83%	c. tallow	0.30	11.46%
red maple	5.95	2.34%	s. tupelo	7.97	4.22%	s. tupelo	34.98	16.82%						
A. elm	1.27	0.50%	red maple	4.23	2.24%	laurel oak	8.67	4.17%						
water elm	0.57	0.22%	ash	1.56	0.82%	red maple	5.63	2.71%						
hornbeam	0.11	0.04%	sweetgum	0.35	0.19%	water oak	2.04	0.98%						
hawthorn	0.05	0.02%	water elm	0.23	0.12%	ash	1.57	0.76%						
						american elm	0.10	0.05%						

All species present are included. Latin binomials are available in Table S1.

Table 2.3. Herbaceous species contributions to standing biomass stocks.

	Nontidal			Head			Upper			Middle			Lower		
Winyah	Species	C (Mg ha^{-1})	%	Species	C (Mg ha^{-1})	%	Species	C (Mg ha^{-1})	%	Species	C (Mg ha^{-1})	%	Species	C (Mg ha^{-1})	%
	panicgrass	0.22	30.62	whitegrass	0.06	68.18	sensitive fern	2.56	19.49	waterparsnip	9.01	22.30	cattail	6.90	23.28
	whitegrass	0.10	13.52	unknown	0.03	31.82	lizards tail	1.85	14.03	giant cutgrass	7.60	18.81	giant cutgrass	3.13	10.56
	beaksedge	0.09	12.10	necromass	0.00	0.00	annual wildrice	1.08	8.20	seaside goldenrod	5.21	12.89	annual wildrice	3.12	10.54
	clearweed	0.05	7.56				halberdleaf	0.74	5.61	annual wildrice	1.99	4.92	softstem bulrush	2.64	8.91
	Elliot's ast.	0.05	7.20				water hemlock	0.73	5.52	water hemlock	1.63	4.03	cordgrass	1.82	6.15
	necromass	0.00	0.00				necromass	0.36	2.73	necromass	1.17	2.90	necromass	5.66	19.11
	Nontidal			Head			Upper			Middle			Lower		
Savannah	Species	C (Mg ha^{-1})	%	Species	C (Mg ha^{-1})	%	Species	C (Mg ha^{-1})	%	Species	C (Mg ha^{-1})	%	Species	C (Mg ha^{-1})	%
	carex	2.32	27.93	panic grass	1.11	22.83	giant cutgrass	2.90	25.52	cattail	2.79	18.30	cordgrass	24.90	34.83
	panicgrass	2.25	27.11	marsh seedbox	0.83	17.07	haspan flatsedge	1.48	13.00	Virginia peltandra	2.33	15.28	giant cutgrass	10.95	15.33
	cordgrass	1.52	18.38	lizards tail	0.80	16.52	cordgrass	1.24	10.87	giant cutgrass	1.65	10.86	cattail	10.80	15.11
	lizards tail	0.86	10.39	s. smartweed	0.67	13.86	panicgrass	1.24	10.91	sturdy bulrush	1.58	10.34	sturdy bulrush	1.76	2.46
	beaksedge	0.75	9.04	seedbox	0.29	5.96	carex	0.64	5.62	lizards tail	0.81	5.31	bur marigold	1.75	2.45
	necromass	0.24	2.92	necromass	0.85	17.56	necromass	0.60	5.24	necromass	0.82	5.38	necromass	19.40	27.14

Only the top 5 species by mass (except where < 5 species were observed) and necromass values in each plot are listed. Latin binomials are available in Table S1.

On all plots, baldcypress (*Taxodium distichum* L. Rich.) and water tupelo (*Nyssa aquatica* L.) dominated the live tree C biomass pools, except for "lower" plots where water tupelo has been excluded by excessive porewater salinity (Table 2.2). Associate species such as swamp tupelo (*Nyssa biflora* Walter), red maple (*Acer rubrum* L), ash (*Fraxinus spp.*), and water elm (*Planera aquatica* J.F. Gmel.) were common, but rarely rose above 10% of overall tree C, with the notable exceptions taking place at the "upper" plots, where moderate stress may be driving higher diversity. Herbaceous C was distributed across a higher number of species with no single species contributing more that 35% of overall yearly C (Table 2.3).

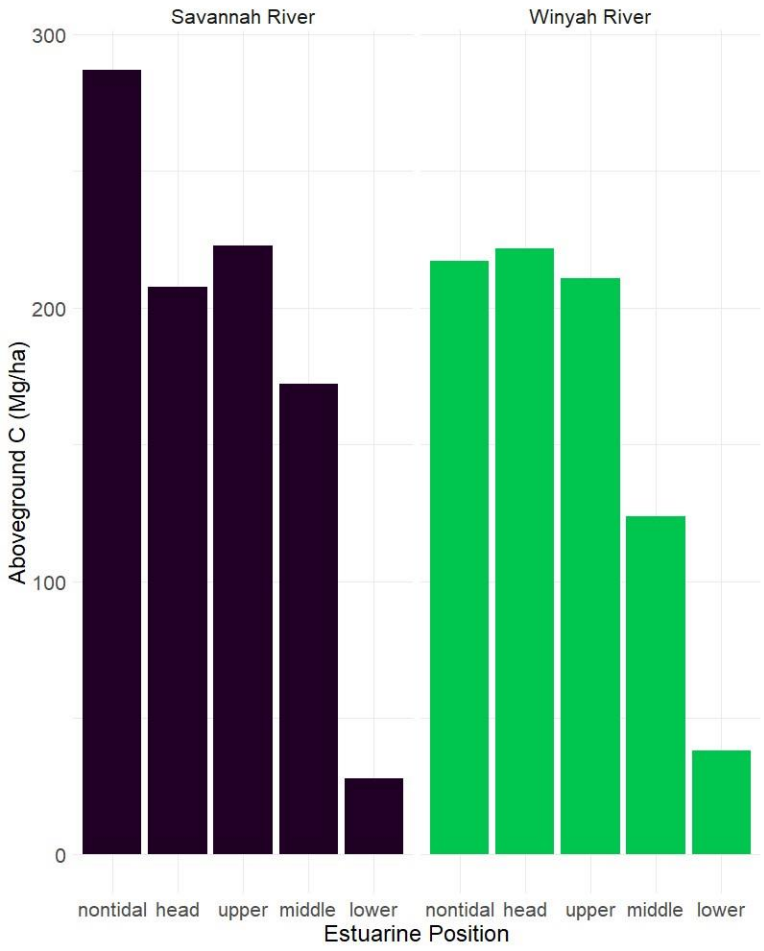

Figure 2.3. Observed aboveground C (Mg ha^{-1}) by estuary position.

In our plots, we observed that herbaceous C pools were negligible in sites approaching the uppermost estuarine extent (nontidal and head-of-tide sites), ranging from 0.0% - 0.26% of non-tree aboveground C in these areas (Figure 2.4). The herbaceous C pool became much more meaningful in the semidiurnal plots towards the seaward side of our estuarine gradient, increasing from 1.7% in continuously freshwater tidal forest (upper sites) to 15.9% in oligohaline tidal forest converting to tidal marsh (lower sites). When CWD and FWD are added together to represent all Downed Woody

Debris (DWD), this pool takes up between 15.4% and 83.9% of non-tree biomass across the estuarine gradient. Sites at the uppermost estuarine extent tended to have more DWD, while seaward estuarine sites showed a higher proportion of their non-tree biomass in still-standing snags. Snags made up 70.2% and 66.4% of non-tree biomass in Winyah and Savannah "lower" sites, respectively. Snags also had large biomass in the "head-of-tide" sites, accounting for 26.2% of non-tree biomass on the Winyah River and 36.3% on the Savannah River. Foliage made up between 3.0% and 32.4% of non-tree biomass in all plots other than Savannah "lower," with this mass unsurprisingly corresponding tightly to tree biomass. Sapling biomass was nearly non-existent in the "lower" and "middle" sites, ranging from 0.0% - 3.1%. This increased in the "upper", "head-of-tide", and "nontidal" sites, where sapling biomass ranged from 6.2% - 27.8% of non-tree C.

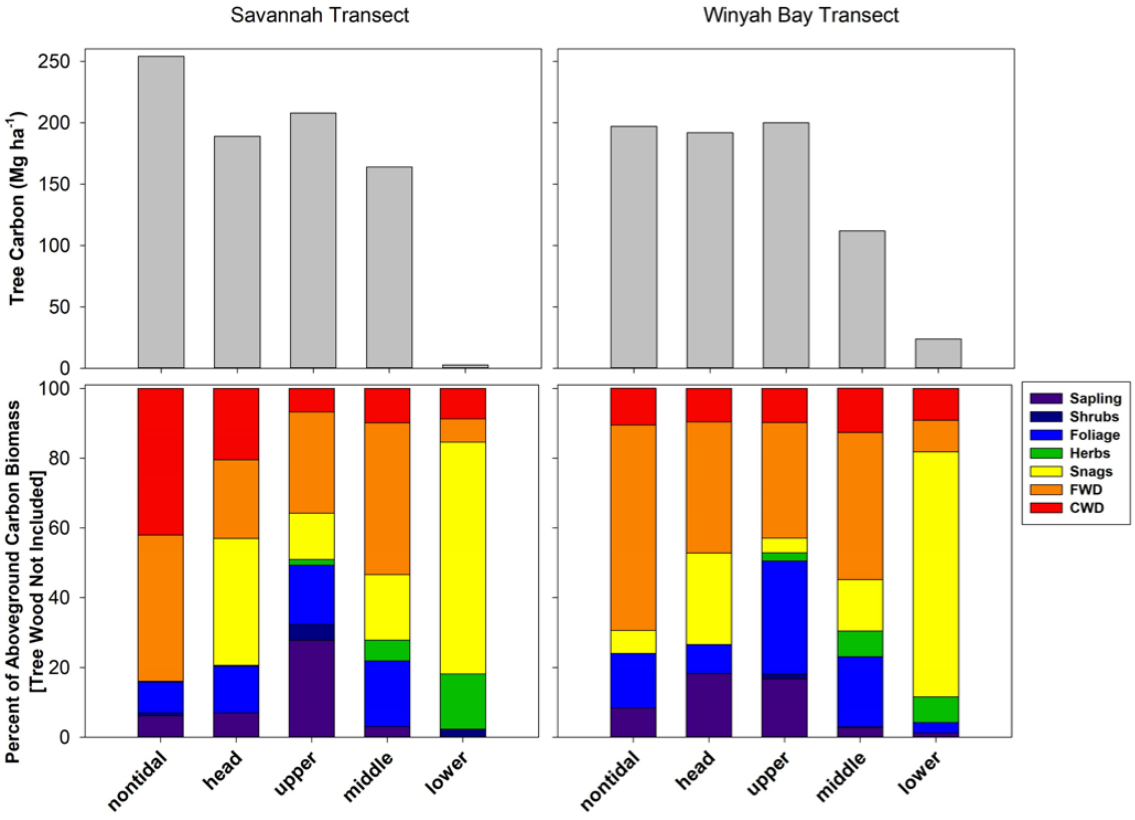

Figure 2.4. (Top) Tree carbon (C) in Megagrams per hectare by river position. (Bottom) Percent contribution of each biomass pool to the given plot's total C, barring live mature trees.

2.4 Discussion

Our analysis of aboveground C along the breadth of UEFWs shows a distinct decrease in standing aboveground C which coincides with salinity intrusion, as our sites approach the critical 2.0 ppt salinity benchmark of complete community transition to tidal marsh (Conner et al., 2007a; Hackney & Avery, 2015; Krauss et al., 2018). Aboveground C stocks drop precipitously at our salt-impacted sites on the seaward side of the estuarine gradient, which follows the expected transition of biomass allocation from mostly

aboveground in upland forests (Houghton et al., 2009) to mostly belowground in marshes (Krauss et al., 2018). Community composition of our sites closely matches the *Taxodium/Nyssa* association described for the Southeastern coastal plains (Conner et al., 2007a).

Total aboveground C stocks across the entire gradient range from 287.0 - 28.1 Mg C ha^{-1}, which are comparable to previous reports of UEFW ecosystems in the southeastern and northwestern United States (Krauss et al., 2018, 184.7 - 5.2 Mg C ha^{-1}; Ricker et al., 2019, 177 - 68.5 Mg C ha^{-1}; Kauffman et al., 2020, 395 - 8.2 Mg C ha^{-1}). For broader comparison, natural forests within the subtropical humid forest ecological zone in North America (*i.e.*, the same zone as our forested wetland study sites) average about 42.3 Mg C ha^{-1} (Shukla et al., 2019). We did not assess belowground C stock in this study but previous work on the same "lower", "middle", and "upper" study sites found that between 56 - 94% of total C is stored belowground in these systems (Krauss et al., 2018).

Comparison of our findings with previous work on the system (Krauss et al., 2018) provide evidence that salinity intrusion of relatively low magnitude (~ 1.0 ppt) can result in meaningful loss of aboveground biomass in UEFW systems. C storage in codominant trees at "middle" plots on both the Winyah and Savannah rivers demonstrated equilibrium (+ 0.8%) or minor losses (- 5.5%), respectively, between 2005 and 2012 when their salinities averaged 1.3 ppt, but growth (+ 19.2%, + 40.2%, resp.) between 2012 and 2020 when relatively fresh (2020-'22 avg = 0.4 ppt) conditions prevailed (Table 2.4). "Lower" sites, which were originally established at the lowest

extent of the UEFW ecological range, were observed to completely transition from forests to oligohaline marshes, with consistent losses of live tree biomass ranging from -22 - 75% over 7-year time steps (Table 2.4) and community composition in 2020 dominated by genera such as *Spartina*, *Typha*, and *Zizaniopsis* (Table 2.3). "Upper" sites on both rivers, which experienced no salinity intrusion, demonstrated highly variable (range from + 6.8% to + 45.7%) but consistently positive (avg = 19.7%) growth across the scope of studies on the system (Table 2.4).

Table 2.4. Comparison of codominant tree C values from Krauss et al. (2018) and the current work.

River	Position	2005 Mg C ha^{-1}		2012 Mg C ha^{-1} (Δ %)		2020 Mg C ha^{-1} (Δ %)
		Interim Salinity (ppt)		*Interim Salinity (ppt)*		
Winyah	Nontidal	n/a		n/a		197.0
	Head	n/a		n/a		192.0
	Upper	128.6	*0.1*	137.3 (+ 6.8%)	*0.07*	200 (+ 45.7%)
	Middle	93.2	*1.4*	93.9 (+ 0.8%)	*0.5*	111.9 (+ 19.2%)
	Lower	49.9	*2.4*	30.6 (- 38.7%)	*1.6*	23.9 (- 21.9%)
Savannah	Nontidal	n/a		n/a		254.1
	Head	n/a		n/a		189.1
	Upper	162.6	*0.1*	187.1 (+ 15.1%)	*0.1*	208.0 (+ 11.2%)
	Middle	123.8	*1.2*	117.0 (- 5.5%)	*0.4*	164.0 (+ 40.2%)
	Lower	42.2	*4.3*	10.8 (- 74.4%)	*3.4*	2.7 (- 75.0%)

Interim salinity values from 2005-2012 are reported from Krauss et al. (2018). Note that 2020 values used height- and diameter-based allometry (Woodall et al., 2011), while previous work used diameter-only equations (Jenkins et al., 2003), which accounts for some of the observed variation.

The expected drivers of the biomass patterns we observed include salinity (Conner et al., 2007b; Krauss et al., 2018) and the concurrent sulfide-induced transition from a methanogenic soil condition to a sulphate-reducing condition (Hackney & Avery, 2015). Soil condition and porewater salinity have been shown to have significant impacts

on not only overall stand density and community (Davis et al., 1981), but also resource partitioning by plants under stress (Allen et al., 1996; Conner & Inabinette, 2005). Freshwater swamps, as well as other floodplains, have been found to contain more dead woody debris than upland forests (Lininger et al., 2017; Ricker et al., 2019) which may drive additional C storage in these systems.

Classification of small woody stems into either shrubs or saplings is often an opaque process, and a noted source of discrepancy between researchers (Heath et al., 2009). The FIA methodology presents a list of shrub species of the US, but researchers are left unclear on what to do with species which exhibit typical shrub characteristics but are not present in that list (*e.g.*, *Morella cerifera* L., *Gaultheria shallon* Pursh). In this study, individual stems were classified as either shrub or sapling based on diameter alone. While this results in some very small saplings being treated as shrubs and some large specimens of stereotypical shrubs being treated as saplings, it is necessitated by the fact that the equations used for our smallest specimens (shrubs) are calibrated for relatively small DBH (< 2.5cm) values, while sapling and tree equations do not function when DBH inputs are under their intended cutoff values (12.5 and 2.5 cm DBH, respectively) (Heath et al., 2009). This will naturally result in the approach-based inter-study discrepancies discussed in Heath et al. (2009), but allowed this study to best estimate our own values.

There is significant discussion in the scientific community addressing numerous sources of error in allometric modelling (del Río et al., 2016, 2019; Forrester & Pretzsch, 2015; Pretzsch, 2019; Vorster et al., 2020) which are relevant to our study. Trees in our

sites exist along salinity gradients that can cause a reduction in canopy crown size which is associated with lower individual tree water use and growth rates, and are analogous to crown sizes in highly competitive stands (Duberstein et al., 2020). At the same time, study sites impacted by saltwater intrusion also have lower stand diversity and presumably less light competition associated with the greatly reduced canopy coverage (Krauss et al., 2018, Table 1). With decreased stem density we might expect that our monospecific "lower" and "middle" sites will exhibit growth patterns moderated in part by their less diverse neighborhood compared to our upriver sites, where baldcypress are exhibiting competition with other genera. The impact of a tree's competition status on the accuracy of generalized allometric models can be complex, with individuals exhibiting variations in stem, crown, and root allometry (del Río et al., 2019). Forrester and Pretzsh (2015) discuss the implications of using allometric equations which were developed in monoculture stands to scale up from single tree to stand scale estimations, including examples of species displaying errors of up to 100% when comparing *E. grandis* growing in mixed vs monospecific stands. This complex set of environmental variables along the observed gradient almost certainly drive high variability in allometric estimations of our subject trees when compared to examples of these species growing in "standard" conditions with which these equations have been developed (del Río et al., 2016; Vorster et al., 2020; Woodall et al., 2011).

2.5 Conclusion

In conclusion, we observed aboveground C values of between 287.0 and 28.1 Mg C ha^{-1} in UEFW ecosystems of the southeastern United States helping us better understand C cycling patterns in these poorly-quantified ecosystems. The seaward reaches of these estuarine forests ranged greatly in their aboveground C storage, from 222.7 to 28.1 Mg C ha^{-1}, while the higher estuarine sites held between 287.0 and 207.8 Mg C ha^{-1}. Most aboveground C storage occurs in the upper estuarine reaches of UEFW, which are simultaneously the least-documented portions thereof. As sea levels rise, we can predict that these currently nontidal sites will trend towards the conditions observed at the more tidally-influenced freshwater sites. This transition may result in significant mobilization of C currently sequestered within woody biomass and will certainly lead to decreased aboveground C storage, although the latter is likely to be offset by the belowground productivity of more marsh-like ecosystems. A better understanding of these system's role in C storage will be critical to upcoming management decisions and preservation efforts.

CHAPTER THREE

RADIAL AND AZIMUTHAL ATTENUATION IN BALDCYPRESS AND WATER TUPELO IN LONG HYDROPERIOD, LOW SALINITY ENVIRONMENTS OF THE SOUTHEASTERN US

3.1 Introduction

The long hydroperiod which defines southern deepwater swamps of the southeastern United States results in three general forest types which are adapted to this environment: Atlantic white cedar swamps, pondcypress/swamp tupelo swamps, and baldcypress/water tupelo swamps (hereafter, cypress-tupelo) (Conner & Buford, 1998). Dominated by baldcypress (*Taxodium distichum* (L.) Rich.) and water tupelo (*Nyssa aquatica* L.), these cypress-tupelo swamps are especially common where coastal tidal influence meets sustained upland water supply (Krauss et al., 2015) and floodplain drainage is restricted by geomorphic barriers (*e.g.*, oxbow lakes and swales). Because these two species can tolerate the long hydroperiods of deepwater systems, we suspect that they may exhibit similar tree level eco-physiological responses to these routinely flooded conditions, resulting in similar patterns of spatial sap flux partitioning between species despite the physiological differences between diverse taxa (*e.g.*, ring-porous vs diffuse-porous growth structure).

Spatial (*i.e.*, radial or azimuthal) variation in sap flow is thought to be one of the largest sources of plant-level systematic error in sap flow assessments (Merlin et al., 2020), contributing to the large inaccuracies found in comparisons of sap flow derived water use estimates with reference methods (Flo et al., 2019; Steppe et al., 2010; Wilson

et al., 2001). As studies using thermometric sapflow methods (TSM) are nearly universally limited in sample size and thus cannot frequently block by species, the use of ring porosity classifications to predict these spatial variation patterns across taxa has been both common practice and the subject of recent debate in the scientific literature (Berdanier et al., 2016; Flo et al., 2019). Non-, diffuse-, and ring-porous classifications of wood anatomy refer primarily to the size and distribution of vessel elements, but also common anatomical traits (*e.g.*, intertracheid pits, ray tracheids, etc) shared by these classes also dictate the radial pathways of solute and water movement (Kitin et al., 2009; Noshiro & Baas, 1998; Román-Jordán et al., 2017). Vessel diameter (higher in ring- and diffuse-porous trees than in non-porous trees) and density (showing the opposite trend) influence both the absolute rate (Kotowska et al., 2021) and spatial distribution (Berdanier et al., 2016) of sap flow, leading to the putative utility of the porosity classifications which encompass these traits. Wood density and moisture content impact the conduction of heat through stem tissues (Vandegehuchte & Steppe, 2013) and can thus interfere with the calibration of thermal sap flow sensors (Flo et al., 2019), but have been found to be insufficient grouping characteristics for the purposes of predicting sap flow trends (Kotowska et al., 2021).

Sap flow rates within the main stem of trees are typically highest within the outermost layers of cambium tissue (Berdanier et al., 2016; Ford et al., 2004; Poyatos et al., 2007), declining exponentially with depth. This relationship is not universal (James et al., 2003), with differences in large part due to variability in tree ring structure (Berdanier et al., 2016). Baldcypress, being a deciduous gymnosperm in the family *Cupressaceae*,

exhibits the non-porous ring structure (Kitin et al., 2009; Román-Jordán et al., 2017) common across all coniferous trees (Peters et al., 2018), while water tupelo is a diffuse-porous hardwood of the family Nyssaceae (Noshiro & Baas, 1998). Other species of non-porous conifers (*Pinus* spp., Ewers & Oren, 2000; Ford et al., 2004) exhibit relatively gentle, Gaussian attenuation patterns with peak sap flux density occurring below the outermost cambium layers and with flows continuing as deep as 150 mm (Berdanier et al., 2016; Ewers & Oren, 2000; Ford et al., 2004). However, diffuse-porous hardwoods such as *Betula* and *Acer* spp. generally show somewhat steeper attenuation curves, with peaks in sap flow within the first 10 - 15 mm of the cambium (Berdanier et al., 2016). Somewhat paradoxically, recent sap flow studies of baldcypress and water tupelo have shown baldcypress to exhibit more rapid radial attenuation than water tupelo, in direct opposition to the general trend of more rapid attenuation in diffuse-porous than non-porous taxa (Duberstein et al., 2020; Krauss et al., 2015).

Implicit in many assessments of whole-tree water use is the assumption that flow rates are symmetrical throughout the cross-section of a tree stem (Shinohara et al., 2013). Azimuthal (sometimes "circumferential") variation is often unaccounted for (***e.g.***, Ford et al., 2004; James et al., 2003; Krauss et al., 2015; Liu et al., 2017; Molina et al., 2016), with a recent review finding that only 34% of studies in sap flux utilizing thermometric sap flow methods consider azimuthal variation at all (Poyatos et al., 2021). This lack of attention is in spite of numerous authors calling for the increased inclusion of azimuthal variation as a variable of interest (Berdanier et al., 2016; Kume et al., 2012; Oliveras & Llorens, 2001; Peters et al., 2018; Shinohara et al., 2013; Tsuruta et al., 2010; Van de

Wal et al., 2015; cf; Komatsu et al., 2017; Molina et al., 2016). When scaled to stand-level water use estimations, azimuthal variation has been found to account for 16.4 - 21.6% of overall variability (Kume et al., 2012). Understanding and documenting these variance sources across a variety of taxa and habitats is vital to better understanding how plant-based transpiration mediates the hydrologic cycle (Schlesinger & Jasechko, 2014).

All measurements of sap flow rates are subject to variance attributable to environmental conditions such as soil water content (Ford et al., 2004; Krauss et al., 2015; Molina et al., 2016; Oren et al., 1999). When saturated conditions are consistent – a typical situation for southern deepwater swamps – the effect of soil water content can be considered negligible (Oren et al., 2001). This study uses thermal dissipation methods (Granier, 1987) to explore patterns in sap flux density and attenuation in morphologically diverse tree species of southern deepwater swamps with consistent freshwater conditions. Salinity is known to impact water use rates and patterns (Duberstein et al., 2020; Krauss et al., 2015; Krauss & Duberstein, 2010); to better understand these interactions it is important to assess freshwater sites to provide a baseline for comparison. To this end, our goals are 1) to describe and compare radial attenuation curves between tupelo and baldcypress, 2) to describe and compare seasonality effects for each species, and 3) to describe and compare azimuthal variation within these species.

3.2 Methods

Location & timeframe

Located on Hobcaw Barony near Georgetown, SC, our study is housed within Strawberry Swamp (Figure 3.1). Soils belong to the Hobcaw series of fine-loamy, siliceous, thermic, typic Umbraquults (Stuckey, 1982) which are either flooded or saturated year-round, fed by upland runoff. The forest community within the swamp changes along a salinity gradient, with freshwater species such as ash (*Fraxinus spp.*) and sweetgum (*Liquidambar styraciflua L.*) giving way to tupelo (*Nyssa spp.*) and baldcypress (*Taxodium distichum (L.) Rich.*) swamps in higher salinity locations (Liu et al., 2017). Two deployments of sap flow probes were used to collect data for this analysis. The first, from April to September of 2015, assessed radial attenuation and seasonality. The second deployment, which included July to August 2020 and June to August 2021, addressed azimuthal attenuation. Interstitial porewater salinity was measured throughout the duration of the study using 8 monitoring wells which allowed measurement of both shallow (6.5 - 20 cm) and deep (60 - 100 cm) groundwater using a handheld sensor (YSI Inc., Pro30 2011, Yellow Springs, OH, USA). The 2015 salinity measurements from these wells have been reported in preceding studies (Duberstein et al., 2020; Liu et al., 2017), but our second deployment data from 2020 and 2021 are additions to this dataset. Covid-related events impacted our ability to obtain these measurements weekly within 2020, reducing our sample size to 5 measurements in 2020 compared to 18 in 2021. In 2015, the average distance from tree to its associated

monitoring well was 6.4 m (S.D. = 2.8 m), while in 2020/21 the average distance was 7.3 m (S.D. = 4.1 m).

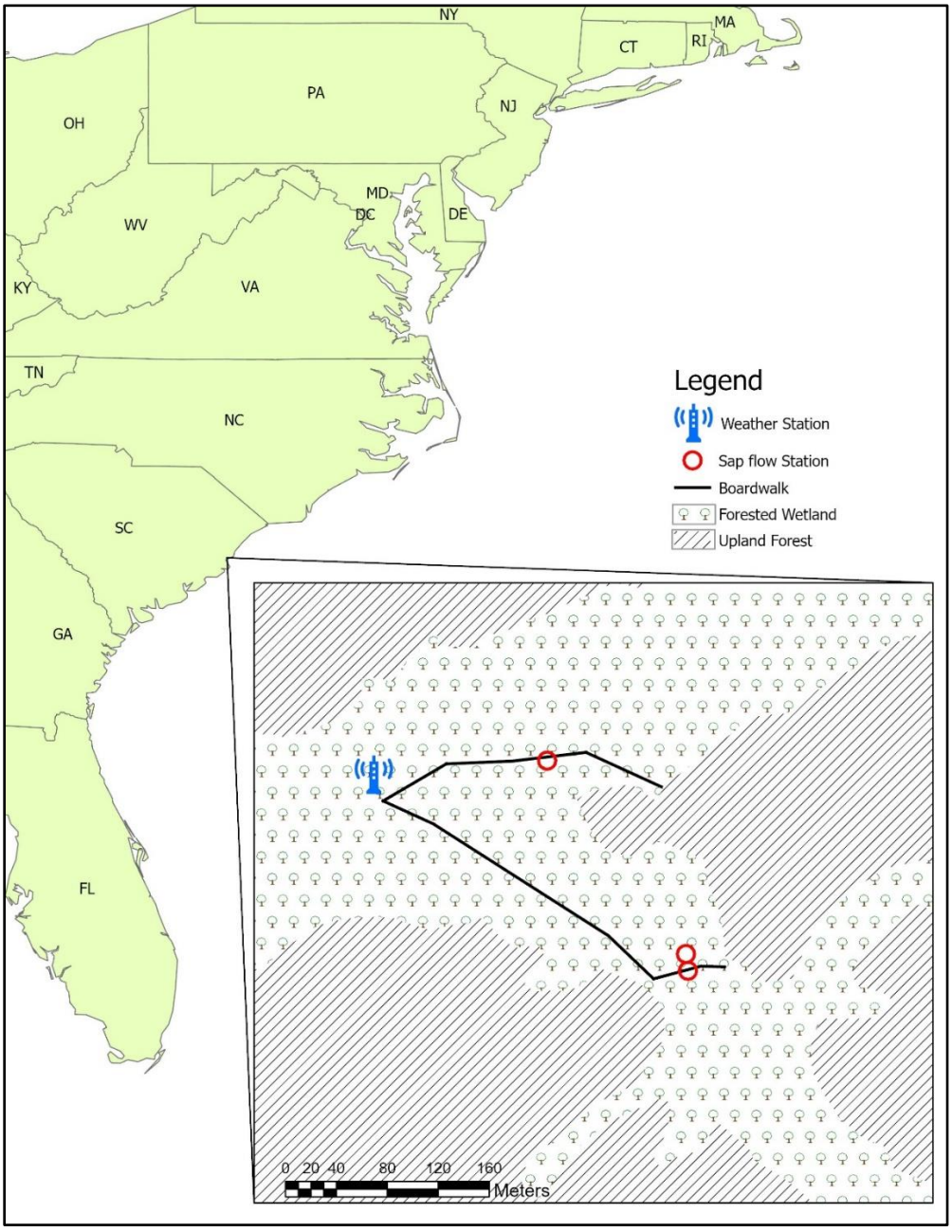

Figure 3.1. Located on Hobcaw Barony in Georgetown County, SC, the study took place in a cypress-tupelo swamp typical of the region. Sap flow and weather station locations remained identical across both deployments.

Sap flow measurements and processing

Across both deployments, Granier-style (Granier, 1987) thermal dissipation sap flow probes (Dynamax Inc., TDP -30, -50, -80, -100, Houston, TX, USA) were installed at data logging stations (Dynamax Inc., FLGS-TDP XM1000, Houston, TX, USA) to instantaneously measure rates of sap flow in 30-min time increments. Only trees which were codominant in the canopy were selected for measurement to control for trees' light competition status. Each probe consists of two vertically aligned needles inserted 4 cm apart (Figure 3.2) which contain thermocouples at identical distances along the needles located at either 15 mm or 25 mm depths; the temperature difference (ΔT) between the paired thermocouples at the same instance provides the means for estimating the rate of flow (Granier, 1987). Flowing sap conducts energy away from the constantly-heated upper probe, decreasing the ΔT between the paired thermocouples inverse to the rate of sap flow in the tree, until a conceivable maximum point at which ΔT equals zero. To minimize measurement error due to external thermal gradients (Lu et al., 2004; Reyes-Acosta et al., 2012), probes were shielded from direct heat from the sun or cooling from rain by the application of reflective mylar shielding attached to the tree, covering the probes (Figure 3.2). Power was supplied to the sap flow units via a bank of 12-V deep cycle marine batteries which were periodically recharged and replaced. Temperature and relative humidity at the base of the live canopy at approximately 7.5 m in height were measured with a weather probe (Vaisala Oyj, HMP45C, Vantaa, Finland) housed within a vented radiation shield mounted on an on-site tower. Weather data were stored on a datalogger (Campbell Scientific Inc., CR800, Logan, Utah). Because vapor pressure

deficit (VPD) is known to be a strong factor effecting tree sap flow, temperature and relative humidity data were used to calculate VPD using the plantecophys package in R (Duursma, 2015).

Figure 3.2. Thermal dissipation probes as deployed in the field in 2020. 4 probes were deployed at 90-degree angles around the tree, aligned with cardinal headings. Mylar shielding was used to protect the probes from rainfall and sunlight which could affect temperature readings.

Measurements of ΔT from the field were processed using the freely available software Baseliner (Oishi et al., 2016), which allows for both automated and visual quality control, as well as the establishment of an environmentally dependent dynamic baseline of zero-flow conditions (Peters et al., 2018). Instantaneous sap flow rates (Js, g m^{-2} sec^{-1}) were calculated according to Krauss et al. (2015) Eq 1;

$$J_s = 119 \times \left(\frac{dT_{\max} - dT_a}{dT_a} \right)^{1.231}$$

where the term in parentheses is equivalent to K, a unitless flow index output by Baseliner (Oishi et al., 2016); dT_{max} is the maximum ΔT measured between the probes during zero-flow conditions, as determined by the moving baseline generated in the Baseliner software; dT_a is the ΔT at a given measurement point in time.

Visual quality control steps for both deployments included the removal of sap flow data exhibiting erratic patterns, as well as the removal of sub-optimal weather as determined by plotting VPD over the duration of the study and removing days with either overall low values (< 1.5 kpa) or sharp drops in VPD indicating rain events during daylight hours. Data were also categorically filtered to only include observations between 10 AM and 7 PM and where Js > 1.0 g m^{-2} sec^{-1}. All statistical analysis was conducted in JMP© Pro, ver 17.1.0.

Radial sap flux monitoring and analysis

Radial sap flux attenuation was assessed using 15 mm-depth sap flux measurements from 15 water tupelo and 15 baldcypress. Of these subjects, 4 water tupelo and 2 baldcypress were fitted with additional probes with thermocouples at a depth of 25 mm, deployed approximately 5 cm above and 5 cm to the left of the 15 mm probe. Two additional water tupelo were outfitted with both 15 and 25 mm probes, but the 15 mm data were entirely removed during quality control, leaving these subjects un-paired. Water tupelo ranged in DBH from 22.3 cm – 50.0 cm (mean 36.5 cm), and baldcypress

ranged from 14.4 cm – 58.3 cm (mean 34.6 cm). 59 days were individually removed due to poor weather conditions after quality control assessments were conducted, reducing our viable days in this deployment from 154 to 95.

Radial attenuation was tested using an REML mixed linear model where individual trees were the subjects of repeated measures over the duration of the first deployment (95 days). The individual tree (nested by species) was also modelled as a random-intercept variable to account for inter-tree variation, which is expected to be high. 30-minute time increments were treated as an ordinal variable, and were modelled as a fixed effect alongside month, species, and sensor depth. A residual covariance structure was used, resulting in a split-plot repeated measures methodology in the JMP modelling framework. Time, species, and depth interaction effects were fully factorial, but model comparison revealed the best fit (lowest AICc; 369,708.41) was achieved when month was not included in any interaction effects. Alternate model constructions with time treated as a random and/or continuous variable did not yield greater model fitness. After this full model was run, data was subset by species and smaller parallel models were constructed to parse the response on a per-species basis. In these subset models, month, time, and sensor depth were included as fixed effects, with all interactions included except the full iteration of the month*time*depth interaction effect, again the result of model comparison. Post-hoc pairwise comparisons of modelled least squares means were conducted on both the full and subset models to assess the nature of fixed and interaction effects using Tukey's HSD tests.

Azimuthal sap flux monitoring and analysis

Azimuthal sap flux patterns were assessed using data from our second round of probe deployments in 2020 and 2021, which were more tightly constrained to the peak summer months to mitigate the effect of seasonality. Data from 2020 spanned Jul - Aug, while 2021 data spanned Jun - Aug. These measurements took place in the same physical locations as the 2015 data, and while resampling of the same trees was not an objective, some study trees were used in both the first and second deployments. Data from 2020 and 2021 are pooled for the purposes of our analysis. Within this deployment, 9 baldcypress and 9 water tupelo trees were fitted with four 15 mm probes each, aligned with the cardinal headings and at 90° angles from one another (Figure 3.2). After assessments for poor weather conditions were conducted, 82 days were individually removed from this deployment reducing our viable days from 152 to 70.

The effect of heading on sap flow rates was statistically modelled in much the same way as radial attenuation. An REML mixed linear model was constructed in which individual trees were the subjects of repeated measures over 70 days, and individual trees (nested within species and by heading) were included as a random-intercept effect in the model. Time, species, and heading were fixed effects, and the fully factorial interaction effects were all included as they showed the best AICc value (272,130.15). A residual covariance structure was used, structuring our analysis as a split-plot repeated measure methodology. The observation month was not included in this model, as this deployment was much more temporally restricted than the previous effort. Post-hoc comparisons of

least square means utilized Tukey's HSD test to assess fixed and interaction effects within the model.

3.3 Results

Environmental measurements

Porewater salinity measurements across both deployments never exceeded 1.8 psu (Table 3.1), but mild salinity intrusion was observed over the course of the 6-year timespan of the two observation efforts. In 2015 the overall average salinity of all wells was 0.5 psu, with a single well reading > 1.0 psu; in 2020-2021 the overall average increased to 0.7, with four wells breaching the 1.0 psu threshold (Table 3.1).

Table 3.1. average salinity measurements across the study duration in Strawberry Swamp, South Carolina, USA.

		2015 avg salinity (psu)		2020-2021 avg salinity(psu)	
	Well	Shallow	Deep	Shallow	Deep
Stand 1	1	0.1	0.3	0.0	0.2
	2	0.4	0.6	0.4	0.5
	3	0.4	0.4	0.3	0.6
	4	0.6	0.7	0.4	0.6
Stand 2	1	0.4	0.7	0.7	0.9
	2	0.4	0.9	0.6	1.0
	3	0.3	0.8	0.5	1.3
	4	0.3	1.3	0.9	1.4

Radial sap flux

Analysis of the data from the first deployment shows an overall difference in Js between species, with an average of 20.7 g m^{-2} sec^{-1} in water tupelo and 24.1 g m^{-2} sec^{-1} in baldcypress, which was found to be significant in post-hoc pairwise analysis of the full

model (Tukey-Kramer adjusted DF = 31.3, f = 13.2, p = 0.001). Subset analysis of each species individually (Figure 3.3) did not show significant differences by depth in water tupelo (21.1 and 19.6 g m^{-2} sec^{-1} at 15 and 25 mm respectively), but in baldcypress sap flow rates at 15mm Js (25.8 g m^{-2} sec^{-1}) were significantly higher than flow rates at 25mm Js (9.5 g m^{-2} sec^{-1}) according to pairwise analysis of modelled LSMeans (Tukey-Kramer adjusted DF = 26062, f = 24.7, $p < 0.0001$). The full model also shows that inter-tree variability accounts for 59.26% of overall model variation ($p = 0.0001$), while subset models by species report that inter-tree variation accounts for 60.4% of variation in water tupelo ($p = 0.005$) and 66.8% of variation in baldcypress ($p = 0.008$). All interaction effects in the full model were found to be significant ($p < 0.05$). Figure 3.4 visualizes the primary finding of the full model, with the significant interaction effect of time by species by depth (f = 18.4, $p < 0.0001$), as well as month as its own fixed effect (f = 3993.7, $p < 0.0001$). Tukey HSD pairwise comparisons of monthly average Js values showed that all months were distinct from one another in the full model, showing a strong effect of seasonality even when our observations are restricted to the growing season (Figure 3.5). Subset modelling of each species' individual monthly response revealed a higher-magnitude seasonal response in water tupelo (LSMean range 12.5 g m^{-2} sec^{-1}) than in baldcypress (LSMean range 8.6 g m^{-2} sec^{-1}). Water tupelo and baldcypress were found to show significantly distinct ($p < 0.001$) patterns of flow throughout the day (Figure 3.6), driven by lower morning and evening flow rates in water tupelo in comparison to baldcypress.

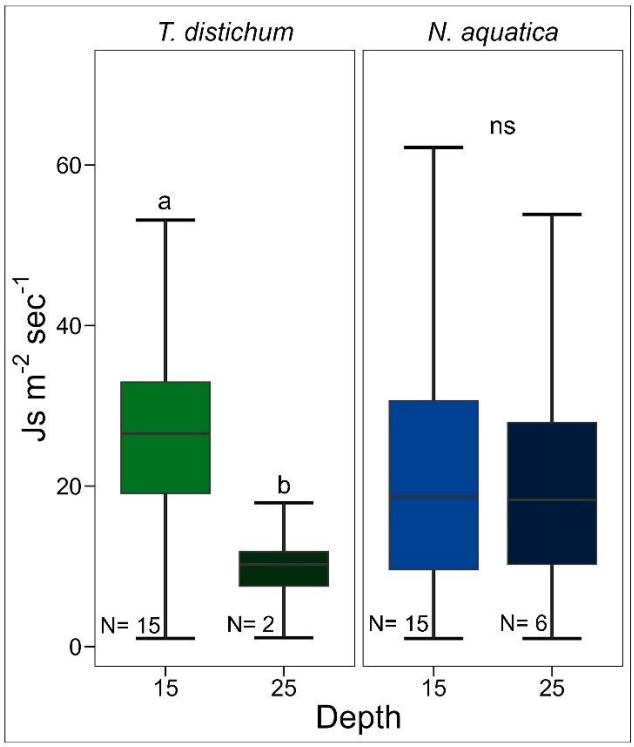

Figure 3.3. Js rates (g m^{-2} sec^{-1}) of water tupelo (*Nyssa aquatica*) and baldcypress (*Taxodium distichum*) trees in Strawberry Swamp. Subset analyses reveal no difference by depth in water tupelo, but differences by depth were significant in baldcypress.

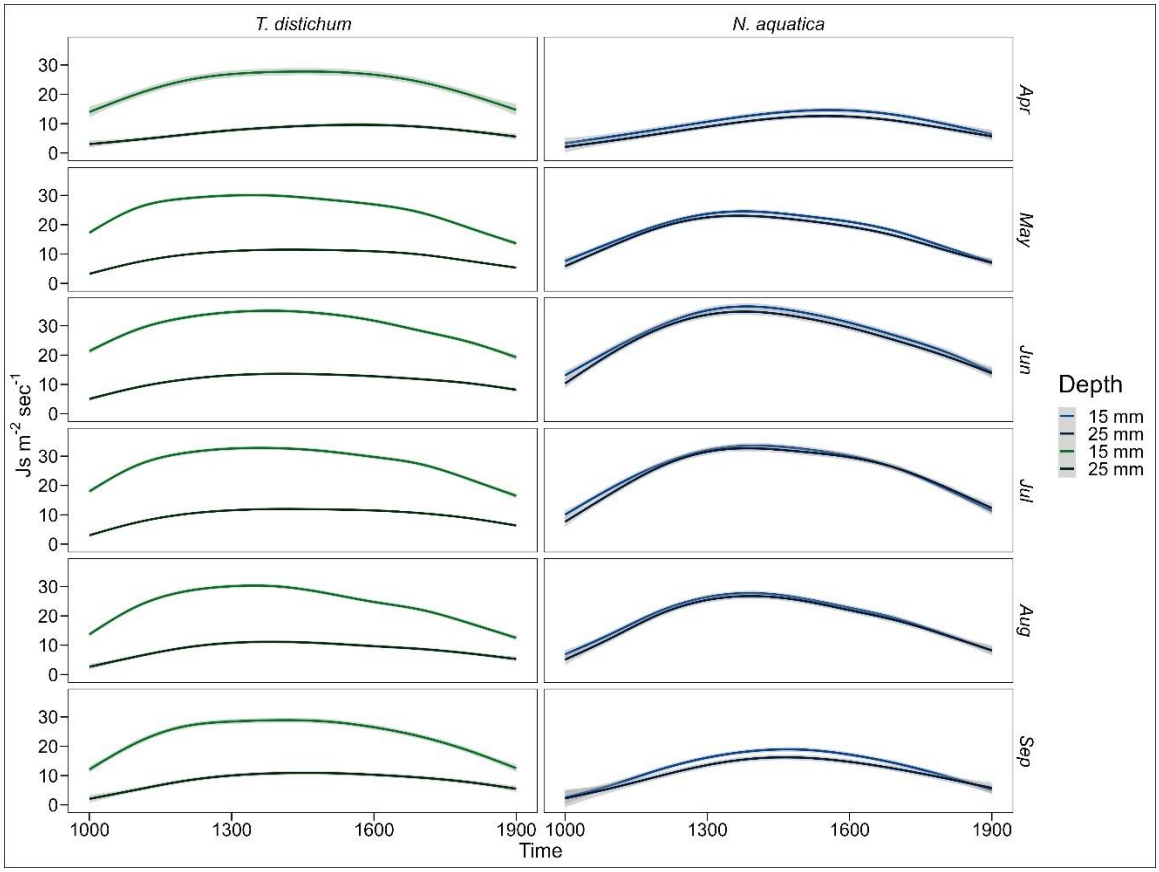

Figure 3.4. Js (g m^{-2} sec^{-1}) patterns of water tupelo (*Nyssa aquatica*) and baldcypress (*Taxodium distichum*) from April to September, at 15 and 25 mm sapwood depths. Error bands represent a 95% confidence interval. Note that the sample size for baldcypress 25 mm depth is only 2, and thus is prone to greater error.

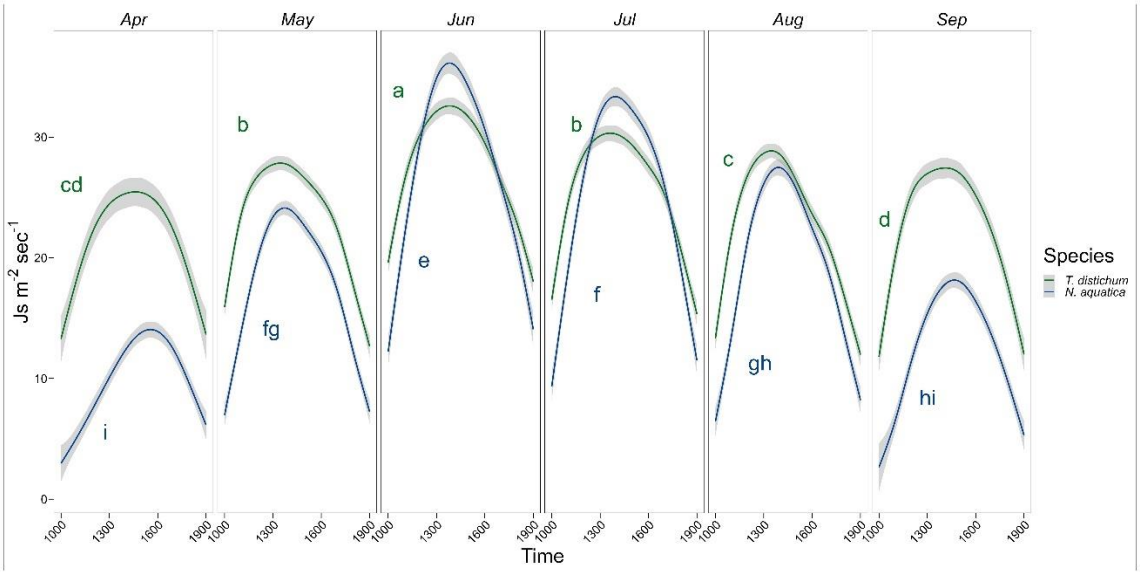

Figure 3.5. Monthly variation in Js (g m^{-2} sec^{-1}) response of water tupelo (*Nyssa aquatica*) and baldcypress (*Taxodium distichum*) trees in Strawberry Swamp. Error bands represent 95% confidence intervals. Letters represent differences according to Tukey's HSD test of subset model LSM estimates, where months sharing a letter are not significantly different from one another. Note that comparisons were not made between species within any given month.

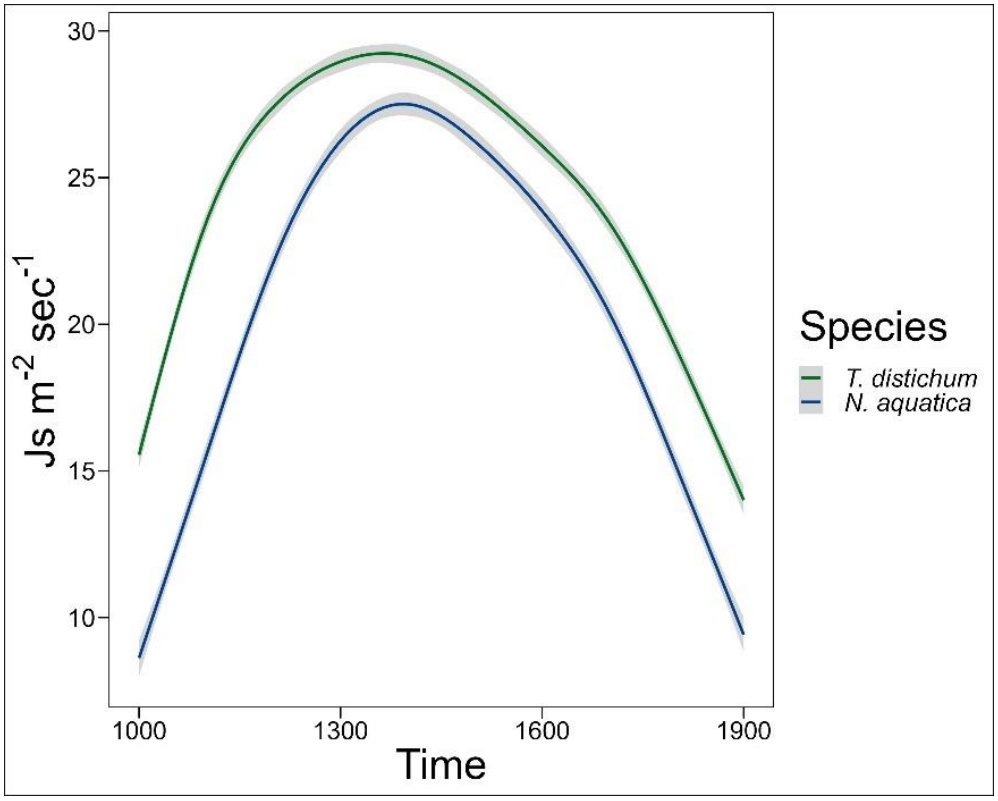

Figure 3.6. Daily Js (g m^{-2} sec^{-1}) patterns of water tupelo (*Nyssa aquatica*) and baldcypress (*Taxodium distichum*), including observations at 15 mm and 25 mm depths. Higher overall Js rates in baldcypress appear to be driven in part by greater flows during morning and evening conditions.

Azimuthal sap flux

Our model assessing the effect of heading on sap flow rates (Figure 3.7) found no significant effect of heading alone, but did find a significant interaction effect between heading, species, and time ($f = 1.94$, $p < 0.0001$). Effects in this model which were repeated from the radial assessment all showed similar results and were all significant ($p < 0.05$). Inter-tree variation within this model accounted for 63.5% of total variation and was significant ($p < 0.0001$).

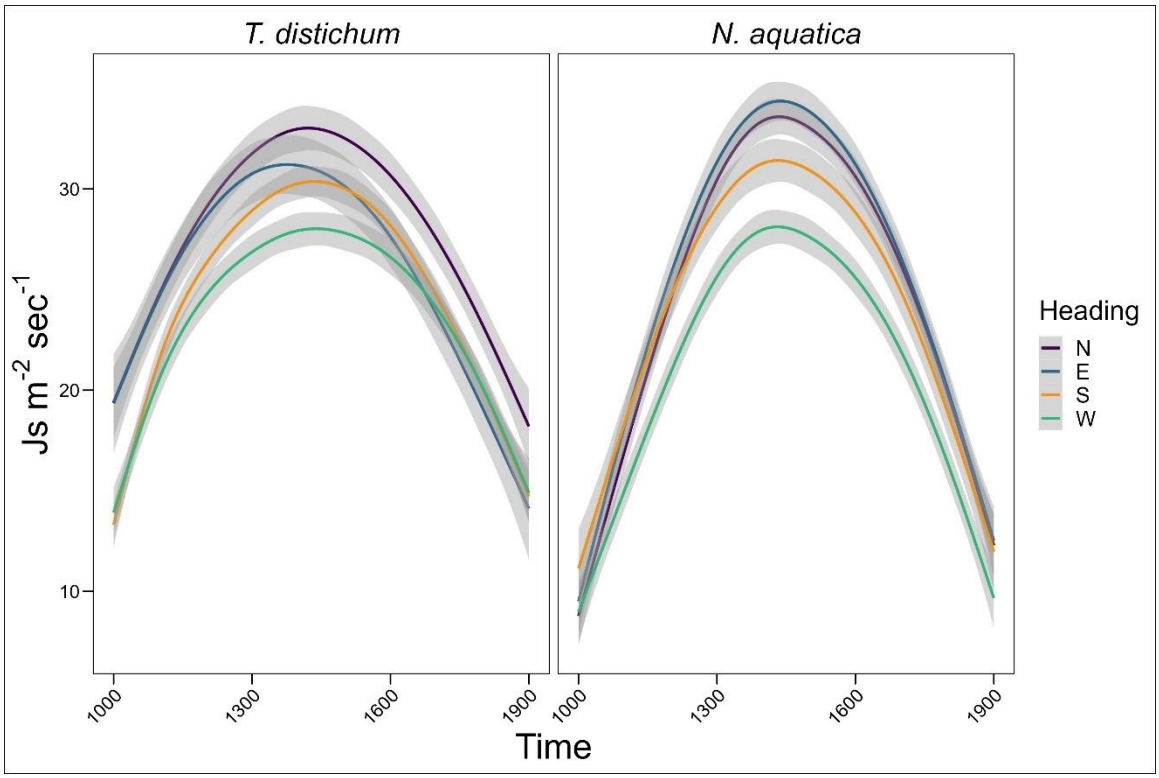

Figure 3.7. Average daily Js (g m^{-2} sec^{-1}) patterns of water tupelo (*Nyssa aquatica*) and baldcypress (*Taxodium distichum*) measured at each cardinal direction around the stem. Error bars represent the 95% confidence interval. N=10 for each combination of species and heading. Heading was not found to be a significant determinant of Js values in this sample.

3.4 Discussion

While recent reviews have found the thermal dissipation method used herein to routinely underestimate (Table 1.3) whole-plant absolute flow values (Flo et al., 2019; Vandegehuchte & Steppe, 2013), it is nonetheless the most common tool used in TSM assessments of sap flux density by far (Peters et al., 2018; Poyatos et al., 2016). Especially in the context of assessing relative sap flow change across spatial or environmental gradients (Flo et al., 2019), the dissipation method is a cost-effective tool with well-developed software applications (*e.g.*, Oishi et al., 2016). The use of these applications to develop and apply an environmentally dependent dynamic baseline has been shown to best account for nighttime sap flow (Peters et al., 2018). The environmental setting and temporal restriction (10 am – 7 pm) of the present study likely mitigates the natural temperature gradients that have long been known to contribute error to TDM studies (Lu et al., 2004), as the strongest impacts have been observed in morning flow values and in semi-arid, open-canopy environments (Reyes-Acosta et al., 2012) which are quite dissimilar to the cypress-tupelo swamps assessed herein.

While radial patterns of sap flux density are thought to be relatively predictable (Berdanier et al., 2016) compared to azimuthal patterns (Komatsu et al., 2017), the radial variation in baldcypress and water tupelo trees remain unresolved. Several investigations of radial attenuation in baldcypress have been conducted (Duberstein et al., 2020; Krauss et al., 2015; Krauss & Duberstein, 2010; Oren et al., 1999, 2001), but those of water tupelo are entirely absent from the literature barring Duberstein et al. (2020), who utilized the same data from 2015 which we expand on herein with the 2020 deployment. The

previous study (Duberstein et al., 2020) resolved sap flow rates at the daily scale and utilized a pre-dawn assessment (*sensu* Peters et al., 2018) of zero-flow conditions, compared to the current use of half-hourly resolution and an environmentally derived assessment of zero-flow conditions. While some authors have argued that a reasonably small sample size can assess this pattern at a species level (Van de Wal et al., 2015), baldcypress have exhibited conflicting patterns in superficially similar environmental conditions. Other studies of baldcypress on identical or comparable sites have reported contradictory patterns in radial sap flow patterns (Table 3.2); flux density was found to be 26% higher in deep xylem than shallow xylem in Duberstein et al. (2013), but Oren et al. (1999) reported that deep xylem (20-40mm sapwood depth) averaged flux densities only ~ 40% of those found in outer xylem.

Table 3.2. Radial patterns observed in archetypal non-porous species and baldcypress (*Taxodium distichum*).

Reference	Species	Environment		Finding	Js_D/Js_S[a]
Berdanier et al. (2016)	*Pinus* & *Tsuga spp*.	Eastern US temperate forests		shallow < deep	n/a[b]
Oren et al. (1999)	*T. distichum*	Freshwater forested wetland	October[c]	shallow = deep	~ 1.0
			August[c]	shallow > deep	0.40
Duberstein et al. (2013)	*T. distichum*	Freshwater forested wetland		shallow < deep	1.26
Present Study[d]	*T. distichum*	Freshwater forested wetland		shallow > deep	0.36[d]
Duberstein et al. (2020)[d]					0.40[d]
Krauss et al. (2015)	*T. distichum*	Forested wetland[e]	Fresh[f]	shallow < deep	1.54
			Saline	shallow > deep	0.61

In all studies shown in Table 3.2, "shallow" refers to sap flux densities within the 0 – 20 mm cambium depth; "deep" refers to densities within the 20 – 40 mm cambium.

[a]: Ratio of deep flow rates (Js_D) over shallow flow rates (Js_S); numbers > 1 represent greater flows in deeper cambium tissues compared to shallow.

[b]: Berdanier et al. (2016) do not report absolute values with which to derive Js_D/Js_S values, but do report peaks in sap flux density values behind the cambium layer (see Figure 3 in Berdanier et al. (2016).

[c]: Oren et al. found divergent radial sapflow trends between the two phases of their study, with insignificant (Student's t, $p > 0.15$) differences by depth in October (during low-flow conditions) but significant differences (Student's t, $p < 0.05$) by depth in August (during high-flow conditions).

[d]: Radial depth findings from this study are derived from the same sap flow observations used in Duberstein et al. (2020), but differential data processing (*e.g.*, ED vs PD zero-flow determination methods) resulted in the slightly divergent Js_D/Js_S observations reported here.

[e]: Values collated by Krauss et al. (2015) span a wide temporal range (2008-2009).

[f]: Fresh observations include both tidal and non-tidal sites; Js_D/Js_S value reported here is average of Js_D/Js_S as shown in Krauss et al. (2015) Table II.

These conflicting findings could potentially result from methodological differences or complex changes in radial patterns over the environmental and temporal gradients that make up the aggregate dataset. Radial patterns have been found to vary in response to both transient environmental drivers (Van de Wal et al., 2015) such as drops in VPD (*i.e.*, precipitation events), as well as chronic drivers such as salinity (Duberstein et al., 2020) in ways that are not yet predictable. Oren et al. (1999) suggested that the two-phase design of their study may not have detected radial differences in October potentially due to lower overall flow rates decreasing the magnitude of the radial pattern, pointing to the additional confounding variable of seasonality atop these trends. It is also possible that the 20 mm depth resolutions reported in the above studies and common throughout the literature are insufficient to resolve the average depth of maximal sap flux in baldcypress; Berdanier et al. (2016) report that this peak may occur somewhere within the first 25 mm of cambium depth in other non-porous conifers, while other studies observe that narrow peak changing depth and magnitude through time (Oren et al., 1999; Van de Wal et al., 2015). This narrow, moving target hypothesis would explain the conflicting findings, both our own and those of other authors, presented in Table 3.2.

Azimuthal variation is much less commonly assessed than radial variation (Kume et al., 2012; Lu et al., 2004; Merlin et al., 2020; Poyatos et al., 2021), and trends have yet to be discerned; while some studies find predictable patterns (*e.g.*, Oren et al., 1999; Tsuruta et al., 2010) possibly influenced by irradiance and crown structure, others find paradoxically opposite (*e.g.*, Van de Wal et al., 2015) or entirely random (*e.g.*, Kume et al., 2012) patterns (Table 3.3). Studies on Japanese cypress (*Chamaecyparis obtusa*

(Sieb. Et Zucc)) and cedar (*Cryptomeria Japonica* (L. f.) D. Don) trees, both of whom are closely related to and share the non-porous wood structure of baldcypress, have found that large variations in azimuthal sap flow patterns can be found at the individual tree level (Sato et al., 2012; Tsuruta et al., 2010), but that these variances are frequently not systematically biased and contribute less to overall uncertainty than between-tree variability components (Komatsu et al., 2017). A similar lack of systemic bias in azimuthal patterns has been found in hardwood species (Komatsu et al., 2017; Merlin et al., 2020; Van de Wal et al., 2015; Wiedemann et al., 2016). Although the magnitude of azimuthal variation may be greater in larger trees, these trends are generally found to be of lower magnitude than radial patterns; this low magnitude may contribute to their erratic appearance throughout the literature (Table 3.3). It is particularly noteworthy that of all the studies presented in (Table 3.3), Oren et al. (1999) is the most directly comparable (taking place in an analogous ecosystem on the same study species), and yet our findings are in direct contradiction; they report flux densities in northern sensors of approximately 64% those found by southeastern and southwestern probes, while we detected no significant difference at all.

Table 3.3. A non-exhaustive collection of studies reporting on the presence (or absence) and directionality of systemic azimuthal sap flow patterns.

Reference	Environment	Species	N	Directionality[a]	Highest Flows
Oren et al. (1999)	Freshwater wetland	*T. distichum*	12	Yes	SE, SW
Tsuruta et al. (2010)	Upland forest	*C. obtusa*	6	Yes	E, S, W
Shinohara et al. (2013)	Upland forest	*C. japonica*	9	Interactive[b]	E, S, W
Van de Wal et al. (2015)	Mangrove forest[c]	*A. marina*	3	Yes	S[c]
Ewers & Oren (2000)	Upland Forest	*P. taeda*	8	No	Equal
Molina et al. (2016)	Irrigated plantation	*P. avium*	6	No	Random
Kume et al. (2012)	Upland forest	*R. pseudoacacia*	3	No	Random
		Q. liaotungensis	3	No	Random
Sato et al. (2012)	Montane forest	*C. obtusa*	3	No	Random
		C. japonica	6	No	Random
Present study	Freshwater wetland	*T. distichum*	9	No	Random
		N. aquatica	9	No	Random

Sample size (N) is reported as the number of replicates per direction included in the study. Species unique to this table include *Pinus taeda* L., *Chamaecyparis obtusa* (Siebold & Zucc.), *Robinia pseudoacacia* L., *Avicennia marina* (Forssk.), *Prunus avium* L., *Quercus liaotungensis* (Koidz.; synonymous with *Q. mongolica* in ITIS database used herein), and *Cryptomeria japonica* (L.f.).

[a]: Refers to the presence of systematically predictable correlations between azimuth and sap flux density.

[b]: Shinohara et al. (2013) did not find significant differences by heading alone, but did report an interaction effect between azimuth and depth.

[c]: Van de Wal et al. (2015) observed only northern and southern aspects. Their study took place in the southern hemisphere, making their finding of higher flows on southern faces somewhat paradoxical.

3.5 Conclusions

Our findings of steeper radial attenuation curves in non-porous baldcypress than in diffuse-porous water tupelo (see Figure 3.3 and Figure 3.4) are in contrast with the established pattern described in the field (*e.g.*, Berdanier et al., 2016), and are not easily reconcilable. These results point to the possibility that the moderation of radial flow patterns by hydraulic characteristics such as vessel diameter and distribution may respond dramatically differently to the environmental drivers found in flooded wetlands, reversing commonly observed patterns. Sap flow studies in wetlands remain sparse (Krauss et al., 2015), potentially contributing to the novelty of these findings.

It has recently been argued that due to the non-directional nature of azimuthal variation findings in the wider literature, it is always better to measure more inter-tree variation than intra-tree variation (Komatsu et al., 2017). Our findings seem to support this, with no strong patterns in azimuthal variation being detected across the breadth of the survey. The inconsistent findings of predictable azimuthal trends (Table 3.3) present an as-yet-unanswered question as to what conditions precipitate irradiance- and structurally-moderated azimuthal patterns, but there is growing evidence that sap flow methodologies should treat azimuthal variation as functionally random (Komatsu et al., 2017; Merlin et al., 2020; Molina et al., 2016). Should this trend continue to develop, it would seem that investigators would be better served placing sensors at random azimuths within a sample of trees rather than following the historic practice of the placement of sensors on the northern face of the tree.

CHAPTER FOUR

SUMMARY AND CONCLUSIONS

Upper estuarine forested wetlands and other coastal wetlands exist in a paradoxical state, being both incredibly valuable in diverse contexts (*i.e.*, playing outsized roles in both C and water cycles compared to their landscape footprints) and less well-quantified than the upland systems they compare so favorably against (Adame et al., 2024). These systems represent some of the most valuable tools in the mitigation of climate change through natural greenhouse gas sequestration, and simultaneously contribute some of the largest uncertainty estimates within our global climatic greenhouse gas and hydrologic modelling efforts (Bar-On et al., 2018; Dix & Aubrey, 2021b). As our ability to manage both C pools and water resources is only predicted to become more urgently critical in the coming years, we hope that the results of our work can contribute to the challenges ahead.

In our review of the broad states of the fields of C inventorying and sap flux-based transpiration estimation, we simultaneously noted the great utility of our current models, as well as the significant outstanding questions and sources of uncertainty. Obviously, international efforts to quantify the C pools and fluxes of the Earth have yielded values which are used globally to inform management decisions (Canadell et al., 2021), but these quantifications also routinely carry error estimates of greater than 100% (Bar-On et al., 2018). While the work of illuminating those sources of error will likely never be complete, the value of our current understanding cannot be understated. Similarly, the field of hydrological modelling via thermometric sapflow methods

provides great insight into the freshwater cycling of our planet, while nonetheless being subject to large outstanding questions (Flo et al., 2019; Poyatos et al., 2021). Across both fields, global collaborations have both provided useful insights on their own merits, as well as contributing to methodological standardization which will contribute to greater precision in and of themselves.

Regarding UEFW C modelling, we assessed aboveground vegetative C stocks and their changes across a river-to-estuary gradient from nontidal and seasonally tidal landscape positions to salinity-impacted freshwater tidal forested wetlands. Standing stocks in these UEFW along the Savannah River in Georgia and the Winyah Bay in South Carolina were evaluated via a space-for-time substitution investigating the impacts on UEFW from relative sea level rise. Aboveground C stocks on these previously poorly quantified systems ranged from 287.0 to 28.1 Mg C ha^{-1}, with average values on the Winyah Bay of 162.3 Mg C ha^{-1}, and average values of 183.6 Mg C ha^{-1} on the Savannah River. Higher-salinity sites analogous to predicted future conditions at the currently fresh sites showed highly variable C stock values, ranging from 222.7 to 28.1 Mg C ha^{-1}, while the landward sites with currently freshwater conditions held between 287.0 and 207.8 Mg C ha^{-1}. Predicted sea level rise models suggest a likely marked decline in C storage on UEFW, potentially paired with significant remobilization of currently sequestered above- and below-ground C stocks (Ensign & Noe, 2018; Wang et al., 2022).

In the field of sap flow-based transpiration estimation, we assessed the radial and azimuthal patterns of sap flow in representative species of non-porous (baldcypress) and diffuse-porous (water tupelo) ring physiologies common to the long-hydroperiod

freshwater swamps of the southeastern United States, suspecting that these taxonomically diverse species may exhibit similar sap flow patterns under permanently flooded conditions. Analysis of our data did not support these hypotheses, with no azimuthal patterns being detected (Figure 3.7), and radial differences between 15 mm and 25 mm depths only present in baldcypress (Figure 3.3). This contradicts the generally observed trend of non-porous trees exhibiting shallower radial attenuation curves. Our sub-daily time series data exhibited high inter-tree variability (accounting for 59.26% of total), supporting the recent argument that experimental designs which prioritize more sample trees may capture more overall variation than those which use the limited probe availability of sap flow studies to capture azimuthal variation (Komatsu et al., 2017). The reversal of common radial attenuation trends (Berdanier et al., 2016) demonstrated herein also implies that the developing use of ring porosity characteristics to predict radial trends may not be generalizable across diverse environments. Our assessment of conflicting findings in both the radial and azimuthal trends reported throughout the literature (Tables 3.2 and 3.3) may warrant concern regarding the spatiotemporal resolutions of current methods and their ability to detect these patterns which appear to shift on scales as fine as individual hours or centimeters. Pilot studies to develop corrective factors for these spatiotemporal patterns as well as empirical calibrations (*e.g.*, Dix & Aubrey, 2021b; Flo et al., 2019) may be needed at the individual site level to close the large uncertainties currently inherent in TSM-based transpiration estimation (Steppe et al., 2010).

APPENDICES

Appendix A

Table S1; extended species reference

Table S1. Common and latin names of all species identified

Common name	Genus	Species	Attribution
alligator weed	Alternanthera	philoxeroides	(Mart.) Griseb
annual wildrice	Zizanea	aquatica	L.
arrowleaf tearthumb	Persicaria	sagittata	(L.) H. Gross
Elliot's aster	Symphyotrichum	elliottii	(Torr. & A. Gray)
perennial saltmarsh aster	Symphyotrichum	tenuifolium	(L.) G.L. Nesom
beaksedge	Rhynchospora	sp	Vahl
bur marigold	Bidens	laevis	(L.) Britton, Sterns & Poggenb.
bladder wort	Utricularia	sp	L.
harlequin blueflag	Iris	versicolor	L.
blue violet	Viola	adunca	Sm.
broadleaf arrowhead	Sagittaria	latifolia	Willd.
bulltongue	Sagittaria	lancifolia	L.
carex	Carex	sp	L.
cattail	Typha	sp	L.
cordgrass	Spartina	sp	Schreb.
giant cutgrass	Zizaniopsis	miliacea	(Michx.) Döll & Asch.
dwarf palmetto	Sabal	minor	(Jacq.) Pers.
smallspike false nettle	Boehmeria	cylindrica	(L.) Sw.
glenwoodgrass	Sacciolepis	indica	(L.) Chase
grassleaf rush	Juncus	marginatus	Rostk.
halberdleaf tearthumb	Persicaria	arifolia	L.
haspan flatsedge	Cyperus	haspan	L.

Table S1 (cont.)

Common name	Genus	Species	Attribution
water hemlock	Cicuta	sp	L.
lanceleaf frogfruit	Phyla	lanceolata	(Michx.) Greene
clearweed	Pilea	sp	Lindl
grasswort	Lilaeopsis	sp	Greene
lizards tail	Saururus	cernuus	L.
love vine	Cuscuta	nevadensis	I.M. Johnst
marsh fleabane	Pluchea	odorata	(L.) Cass.
marsh seedbox	Ludwigia	palustris	(L.) Elliott
dewflower	Murdannia	sp	Royle
panic grass	Panicum	sp	L.
Virginia peltandra	Peltandra	virginica	L.
Manyflower marshpennywort	Hydrocotyle	umbellata	L.
pickerel weed	Pontederia	cordata	L.
eryngo	Eryngium	sp	L.
seaside goldenrod	Solidago	sempervirens	L.
seedbox	Ludwigia	alterniflora	L.
sensitive fern	Onoclea	sensibilis	L.
slenderleaf false dragonshead	Physostegia	leptophylla	Small
softstem bulrush	Schoenoplectus	tabernaemontani	(C.C. Gmel.) Palla
streambank spiderlilly	Hymenocallis	rotata	(Ker Gawl.) Herb.
sand spikerush	Eleocharis	montevidensis	Kunth
sturdy bulrush	Bolboschoenus	robustus	(Pursh) Soják
swamp smartweed	Persicaria	hydropiperoides	(Michx.) Small
tapertip rush	Juncus	acuminatus	Michx.
common waterparsnip	Sium	suave	Walter
whitegrass	Leersia	virginica	Willd.

Table S1 (cont.)

Common name	Genus	Species	Attribution
yelloweyed grass	Xyris	sp	L.
American elm	Ulmus	americana	L.
American hornbeam	Carpinus	caroliniana	Walter
ash	Fraxinus	sp	L.
baldcypress	Taxodium	distichum	(L.) Rich.
Chinese tallow	Triadica	sebifera	(L.) Small
possumhaw	Ilex	decidua	Walter
hawthorn	Crataegus	sp	L.
laurel oak	Quercus	laurifolia	Michx.
red maple	Acer	rubrum	L.
swamp cottonwood	Populus	heterophylla	L.
swamp tupelo	Nyssa	biflora	Walter
sweetgum	Liquidambar	styraciflua	L.
water elm	Planera	aquatica	J.F. Gmel.
water oak	Quercus	nigra	L.
water tupelo	Nyssa	aquatica	L.
waxmyrtle	Morella	cerifera	(L.) Small
white oak	Quercus	alba	L.
American holly	Ilex	opaca	Aiton
baccharis	Baccharis	sp	L.
buttonbush	Cephalanthus	occidentalis	L.
English holly	Ilex	aquifolium	L.
flowering dogwood	Cornus	florida	L.
hazel alder	Alnus	serrulata	(Aiton) Willd.
inkberry	Ilex	glabra	(L.) A. Gray
common persimmon	Diospyros	virginiana	L.

Table S1 (cont.)

Common name	Genus	Species	Attribution
swamp bay	Persea	palustris	(Raf.) Sarg.
swamp dogwood	Cornus	foemina	Mill.
swamp-locust	Gleditsia	aquatica	Marshall
swamp white oak	Quercus	bicolor	Willd.

Scientific names retrieved [18-Apr-2024] from the Integrated Taxonomic Information System (ITIS; www.itis.gov, CC0, https://doi.org/10.5066/F7KH0KBK

REFERENCES

Adame, M. F., Kelleway, J., Krauss, K. W., Lovelock, C. E., Adams, J. B., Trevathan-Tackett, S. M., Noe, G., Jeffrey, L., Ronan, M., Zann, M., Carnell, P. E., Iram, N., Maher, D. T., Murdiyarso, D., Sasmito, S., Tran, D. B., Dargusch, P., Kauffman, J. B., & Brophy, L. (2024). All tidal wetlands are blue carbon ecosystems. *BioScience*. https://doi.org/10.1093/biosci/biae007

Allen, J. A., Pezeshki, S. R., & Chambers, J. L. (1996). Interaction of flooding and salinity stress on baldcypress (*Taxodium distichum*). *Tree Physiology*, *16*, 307–313.

Allen, C. D., Breshears, D. D., & McDowell, N. G. (2015). On underestimation of global vulnerability to tree mortality and forest die-off from hotter drought in the Anthropocene. *Ecosphere*, *6*(8). https://doi.org/10.1890/ES15-00203.1

Anderson-Teixeira, K. J., Wang, M. M. H., Mcgarvey, J. C., Herrmann, V., Tepley, A. J., Bond-Lamberty, B., & Lebauer, D. S. (2018). ForC: a global database of forest carbon stocks and fluxes. *Data Papers Ecology*, *99*(6), 1507. https://doi.org/10.5061/dryad.t516f

Barbier, E. B., Hacker, S. D., Kennedy, C., Koch, E. W., Stier, A. C., & Silliman, B. R. (2011). The value of estuarine and coastal ecosystem services. In *Ecological Monographs* (Vol. 81, Issue 2, pp. 169–193). https://doi.org/10.1890/10-1510.1

Barendregt, A., Whigham, D. F., & Baldwin, A. H. (2009). Chapter 18 - Tidal Freshwater Wetlands. In *Coastal Wetlands: An Integrated Ecosystem Approach* (First edit). Elsevier. https://www.sciencedirect.com/science/article/pii/B9780444638939000186

Bar-On, Y. M., Phillips, R., & Milo, R. (2018). The biomass distribution on Earth. *Proceedings of the National Academy of Sciences of the United States of America*, *115*(25), 6506–6511. https://doi.org/10.1073/pnas.1711842115

Berdanier, A. B., Miniat, C. F., & Clark, J. S. (2016). Predictive models for radial sap flux variation in coniferous, diffuse-porous and ring-porous temperate trees. *Tree Physiology*, *36*(8), 932–941. https://doi.org/10.1093/treephys/tpw027

Bridgham, S. D., Megonigal, J. P., Keller, J. K., Bliss, N. B., & Trettin, C. (2006). The carbon balance of North American wetlands. *Wetlands*, *26*(4), 889–916. https://doi.org/10.1672/0277-5212(2006)26[889:TCBONA]2.0.CO;2

Brophy, L. S. (2019). *Comparing historical losses of forested, scrub-shrub, and emergent tidal wetlands on the Oregon coast, USA: A paradigm shift for estuary restoration and conservation Comparing historical losses of forested, scrub-shrub and emergent tidal wetlands on the Oregon coast, USA: A paradigm shift for estuary conservation and restoration*. https://appliedeco.org/report/brophy_2019_oregon_tidal_swamp_and_marsh_losses_final_dec2019/

Canadell, J. G., Monteiro, P. M. S., Costa, M. H., Cotrim da Cunha, L., Cox, P. M., Eliseev, A. V., Henson, S., Ishii, M., Jaccard, S., Koven, C., Lohila, A., Patra, P. K., Piao, S., Rogelj, J., Syampungani, S., Zaehle, S., & Zickfield, K. (2021). Global Carbon and Other Biogeochemical Cycles and Feedbacks. In *Climate Change 2021 – The Physical Science Basis* (pp. 673–816). Cambridge University Press. https://doi.org/10.1017/9781009157896.007

Čermák, J., Jeník, J., Kučera, J., & Žídek, V. (1984). Xylem water flow in a crack willow tree in relation to diurnal changes of environment. *Oecologia*, *64*(2), 145–151.

Chaturvedi, R. K., & Raghubanshi, A. S. (2013). Aboveground biomass estimation of small diameter woody species of tropical dry forest. *New Forests*, *44*(4), 509–519. https://doi.org/10.1007/s11056-012-9359-z

Chave, J., Réjou-Méchain, M., Búrquez, A., Chidumayo, E., Colgan, M. S., Delitti, W. B. C., Duque, A., Eid, T., Fearnside, P. M., Goodman, R. C., Henry, M., Martínez-Yrízar, A., Mugasha, W. A., Muller-Landau, H. C., Mencuccini, M., Nelson, B. W., Ngomanda, A., Nogueira, E. M., Ortiz-Malavassi, E., … Vieilledent, G. (2014). Improved allometric models to estimate the aboveground biomass of tropical trees. *Global Change Biology*, *20*(10), 3177–3190. https://doi.org/10.1111/gcb.12629

Chmura, G. L., Anisfeld, S. C., Cahoon, D. R., & Lynch, J. C. (2003). Global carbon sequestration in tidal, saline wetland soils. *Global Biogeochemical Cycles*, *17*(4), n/a-n/a. https://doi.org/10.1029/2002gb001917

Chu, C. R., Hsieh, C. I., Wu, S. Y., & Phillips, N. G. (2009). Transient response of sap flow to wind speed. *Journal of Experimental Botany*, *60*(1), 249–255. https://doi.org/10.1093/jxb/ern282

Clearwater, M. J., Luo, Z., Mazzeo, M., & Dichio, B. (2009). An external heat pulse method for measurement of sap flow through fruit pedicels, leaf petioles and other small-diameter stems. *Plant, Cell and Environment*, *32*(12), 1652–1663. https://doi.org/10.1111/j.1365-3040.2009.02026.x

Clearwater, M. J., Meinzer, F. C., Andrade, J. L., Goldstein, G., & Holbrook, N. M. (1999). Potential errors in measurement of nonuniform sap flow using heat dissipation probes. *Tree Physiology*, *19*(10), 681–687. https://doi.org/10.1093/treephys/19.10.681

Clough, B. J., Russell, M. B., Domke, G. M., Woodall, C. W., & Radtke, P. J. (2016). Comparing tree foliage biomass models fitted to a multispecies, felled-tree biomass dataset for the United States. *Ecological Modelling*, *333*, 79–91. https://doi.org/10.1016/j.ecolmodel.2016.04.009

Conner, W., & Buford, M. A. (1998). Southern Deepwater Swamps. In M. G. Messina & W. H. Conner (Eds.), *Southern Forested Wetlands* (pp. 261–287). Lewis Publishers. https://tigerprints.clemson.edu/ag_pubs

Conner, W. H., & Inabinette, L. W. (2005). *Identification of salt tolerant baldcypress (Taxodium distichum (L .) Rich) for planting in coastal areas*. 305–312. https://doi.org/10.1007/s11056-005-5658-y

Conner, W. H., Doyle, T. W., & Krauss, K. W. (2007a). *Ecology of Tidal Freshwater Forested Wetlands of the Southeastern United States* (1st ed.). Springer Netherlands. https://doi.org/10.1007/978-1-4020-5095-4

Conner, W. H., Krauss, K. W., & Doyle, T. W. (2007b). Ecology of tidal freshwater forests in Coastal Deltaic Louisiana and Northeastern South Carolina. In W. H. Conner, T. W. Doyle, & K. W. Krauss (Eds.), *Ecology of Tidal Freshwater Forested Wetlands of the Southeastern United States* (pp. 223–253). https://doi.org/10.1007/978-1-4020-5095-4_9

Craft, C., Clough, J., Ehman, J., Jove, S., Park, R., Pennings, S., Guo, H., & Machmuller, M. (2009). Forecasting the effects of accelerated sea-level rise on tidal marsh ecosystem services. *Frontiers in Ecology and the Environment*, *7*(2), 73–78. https://doi.org/10.1890/070219

da Rosa Ferraz Jardim, A. M., de Morais, J. E. F., de Souza, L. S. B., & da Silva, T. G. F. (2022). Understanding interactive processes: a review of CO_2 flux, evapotranspiration, and energy partitioning under stressful conditions in dry forest and agricultural environments. In *Environmental Monitoring and Assessment* (Vol. 194, Issue 10). Springer Science and Business Media Deutschland GmbH. https://doi.org/10.1007/s10661-022-10339-7

Davidson, N. C. (2014). How much wetland has the world lost? Long-term and recent trends in global wetland area. *Marine and Freshwater Research*, *65*(10), 934–941. https://doi.org/10.1071/MF14173

Davis, D., DeRouen, M., Roberts, D., & Wicker, K. (1981). *Assessment of extent and impact of saltwater intrusion into the wetlands of Tangipahoa Parish, Louisiana* (p. 59). Coastal Environments, Inc.

Day, F. P., & Monk, C. D. (1974). Vegetation patterns on a southern Appalachian watershed. *Ecology*, *55*(5), 1064–1074. http://www.jstor.org/stable/1940356?seq=1&cid=pdf-reference#references_tab_contents

del Río, M., Bravo-Oviedo, A., Ruiz-Peinado, R., & Condés, S. (2019). Tree allometry variation in response to intra- and inter-specific competitions. *Trees - Structure and Function*, *33*(1), 121–138. https://doi.org/10.1007/s00468-018-1763-3

del Río, M., Pretzsch, H., Alberdi, I., Bielak, K., Bravo, F., Brunner, A., Condés, S., Ducey, M. J., Fonseca, T., von Lüpke, N., Pach, M., Peric, S., Perot, T., Souidi, Z., Spathelf, P., Sterba, H., Tijardovic, M., Tomé, M., Vallet, P., & Bravo-Oviedo, A. (2016). Characterization of the structure, dynamics, and productivity of mixed-species stands: review and perspectives. *European Journal of Forest Research*, *135*(1), 23–49. https://doi.org/10.1007/s10342-015-0927-6

Dix, M. J., & Aubrey, D. P. (2021a). Calibration approach and range of observed sap flow influences transpiration estimates from thermal dissipation sensors. *Agricultural and Forest Meteorology*, *307*. https://doi.org/10.1016/j.agrformet.2021.108534

Dix, M. J., & Aubrey, D. P. (2021b). Recalibrating best practices, challenges, and limitations of estimating tree transpiration via sap flow. *Current Forestry Reports*, *7*(1), 31–37. https://doi.org/10.1007/s40725-021-00134-x

Dixon, H. H. (1914). *Transpiration and the ascent of sap in plants*. Macmillan and Company, limited.

Domke, G. M., Woodall, C. W., & Smith, J. E. (2011). Accounting for density reduction and structural loss in standing dead trees: Implications for forest biomass and carbon stock estimates in the United States. *Carbon Balance and Management*, *6*, 1–11. https://doi.org/10.1186/1750-0680-6-14

Domke, G., Brandon, A., Diaz-Lasco, R., Federici, S., Garcia-Apaza, E., Grassi, G., Gschwantner, T., Herold, M., Hirata, Y., Kasimir, Å., James Kinyanjui, M., Krisnawati, H., Lehtonen, A., Malimbwi, R. E., Niinistö, S., Michael Ogle, S., Paul, T., Ravindranath, N. H., Rock, J., … Verchot, L. (2019). 2019 Refinement to the 2006 IPCC Guidelines for National Greenhouse Gas Inventories: Agriculture, Forestry and Other Land Use. In *IPCC* (Vol. 4).

Donato, D. C., Kauffman, J. B., Murdiyarso, D., Kurnianto, S., Stidham, M., & Kanninen, M. (2011). Mangroves among the most carbon-rich forests in the tropics. *Nature Geoscience*, *4*(5), 293–297. https://doi.org/10.1038/ngeo1123

Doyle, T. W., O'Neil, C. P., Melder, M. P. V., From, A. S., & Palta, M. M. (2007). Tidal freshwater swamps of the southeastern United States: Effects of land use, hurricanes, sea-level rise, and climate change. In W. H. Conner, T. W. Doyle, & K. W. Krauss (Eds.), *Ecology of Tidal Freshwater Forested Wetlands of the Southeastern United States* (pp. 1–28). Springer Netherlands. https://doi.org/10.1007/978-1-4020-5095-4_1

Duarte, C. M., Losada, I. J., Hendriks, I. E., Mazarrasa, I., & Marbà, N. (2013). The role of coastal plant communities for climate change mitigation and adaptation. *Nature Climate Change*, *3*(11), 961–968. https://doi.org/10.1038/nclimate1970

Duberstein, J. A., Conner, W. H., & Krauss, K. W. (2014). Woody vegetation communities of tidal freshwater swamps in South Carolina, Georgia and Florida (US) with comparisons to similar systems in the US and South America. *Journal of Vegetation Science*, *25*(3), 848–862. https://doi.org/10.1111/jvs.12115

Duberstein, J. A., Krauss, K. W., Baldwin, M. J., Allen, S. T., Conner, W. H., Salter, J. S., & Miloshis, M. (2020). Small gradients in salinity have large effects on stand water use in freshwater wetland forests. *Forest Ecology and Management*, *473*(February), 118308. https://doi.org/10.1016/j.foreco.2020.118308

Duberstein, J. A., Krauss, K. W., Conner, W. H., Bridges, W. C., & Shelburne, V. B. (2013). Do hummocks provide a physiological advantage to even the most flood tolerant of tidal freshwater trees? *Wetlands*, *33*(3), 399–408. https://doi.org/10.1007/s13157-013-0397-x

Dujesiefken, D., Rhaesa, A., Eckstein, D., & Stobbe, H. (1999). Tree wound reactions of Differently Treated Boreholes. *Journal of Arboriculture*, *25*(3).

Duursma, R. A. (2015). Plantecophys - An R package for analysing and modelling leaf gas exchange data. *PLoS ONE*, *10*(11). https://doi.org/10.1371/journal.pone.0143346

Ensign, S. H., & Noe, G. B. (2018). Tidal extension and sea-level rise: recommendations for a research agenda. *Frontiers in Ecology and the Environment*, *16*(1), 37–43. https://doi.org/10.1002/fee.1745

Ensign, S. H., Hupp, C. R., Noe, G. B., Krauss, K. W., & Stagg, C. L. (2014). Sediment accretion in tidal freshwater forests and oligohaline marshes of the Waccamaw and Savannah rivers, USA. *Estuaries and Coasts*, *37*(5), 1107–1119. https://doi.org/10.1007/s12237-013-9744-7

Erb, K. H., Kastner, T., Plutzar, C., Bais, A. L. S., Carvalhais, N., Fetzel, T., Gingrich, S., Haberl, H., Lauk, C., Niedertscheider, M., Pongratz, J., Thurner, M., & Luyssaert, S. (2018). Unexpectedly large impact of forest management and grazing on global vegetation biomass. *Nature*, *553*(7686), 73–76. https://doi.org/10.1038/nature25138

Ewers, B. E., & Oren, R. (2000). Analyses of assumptions and errors in the calculation of stomatal conductance from sap flux measurements. *Tree Physiology*, *20*(9), 579–589. https://doi.org/10.1093/treephys/20.9.579

Fan, J., Guyot, A., Ostergaard, K. T., & Lockington, D. A. (2018). Effects of earlywood and latewood on sap flux density-based transpiration estimates in conifers. *Agricultural and Forest Meteorology*, *249*, 264–274. https://doi.org/10.1016/j.agrformet.2017.11.006

Feagin, R. A., Forbrich, I., Huff, T. P., Barr, J. G., Ruiz-Plancarte, J., Fuentes, J. D., Najjar, R. G., Vargas, R., Vázquez-Lule, A., Windham-Myers, L., Kroeger, K. D., Ward, E. J., Moore, G. W., Leclerc, M., Krauss, K. W., Stagg, C. L., Alber, M., Knox, S. H., Schäfer, K. V. R., … Miao, G. (2020). Tidal wetland gross primary production across the continental United States, 2000–2019. *Global Biogeochemical Cycles*, *34*(2), 1–25. https://doi.org/10.1029/2019GB006349

Field, D. W., Reyer, A. J., Genovese, P. V, & Shearer, B. D. (1991). Coastal Wetlands of the United States: An Accounting of a Valuable National Resource. In *Oxford University* (p. 60). National Oceanic and Atmospheric Administration.

Flo, V., Martinez-Vilalta, J., Steppe, K., Schuldt, B., & Poyatos, R. (2019). A synthesis of bias and uncertainty in sap flow methods. *Agricultural and Forest Meteorology*, *271*(March), 362–374. https://doi.org/10.1016/j.agrformet.2019.03.012

Fonseca, W., Alice, F. E., & Rey-Benayas, J. M. (2012). Carbon accumulation in aboveground and belowground biomass and soil of different age native forest plantations in the humid tropical lowlands of Costa Rica. *New Forests*, *43*(2), 197–211. https://doi.org/10.1007/s11056-011-9273-9

Ford, C. R., Goranson, C. E., Mitchell, R. J., Will, R. E., & Teskey, R. O. (2004). Diurnal and seasonal variability in the radial distribution of sap flow: predicting total stem flow in Pinus taeda trees. *Tree Physiology*, *24*(9), 951–960. https://doi.org/10.1093/treephys/24.9.951

Forrester, D. I., & Pretzsch, H. (2015). Tamm Review : On the strength of evidence when comparing ecosystem functions of mixtures with monocultures. Forest Ecology and Management, *356*, 41–53. https://doi.org/10.1016/j.foreco.2015.08.016

Friedlingstein, P., O'Sullivan, M., Jones, M. W., Andrew, R. M., Hauck, J., Olsen, A., Peters, G. P., Peters, W., Pongratz, J., Sitch, S., Le Quéré, C., Canadell, J. G., Ciais, P., Jackson, R. B., Alin, S., Aragão, L. E. O. C., Arneth, A., Arora, V., Bates, N. R., … Zaehle, S. (2020). Global carbon budget 2020. *Earth System Science Data*, *12*(4), 3269–3340. https://doi.org/10.5194/essd-12-3269-2020

Goldsmith, G. R. (2013). Changing directions: the atmosphere-plant-soil continuum. *Source: The New Phytologist*, *199*(1), 4–6. https://doi.org/10.2307/newphytologist.199.1.4

Granier, A. (1987). Evaluation of transpiration in a Douglas-fir stand by means of sap flow measurements. *Tree Physiology*, *3*(4), 309–320. https://doi.org/10.1093/treephys/3.4.309

Green, S., Clothier, B., & Perie, E. (2009). A re-analysis of heat pulse theory across a wide range of sap flows. *Acta Horticulturae*, *846*, 95–104. https://doi.org/10.17660/ActaHortic.2009.846.8

Hackney, C. T., & Avery, G. B. (2015). Tidal wetland community response to varying levels of flooding by saline water. *Wetlands*, *35*(2), 227–236. https://doi.org/10.1007/s13157-014-0597-z

Heath, L. S., Hansen, M. H., Smith, J. E., Smith, B. W., & Miles, P. D. (2009). Investigation into calculating tree biomass and carbon in the FIADB using a biomass expansion factor approach. In: McWilliams W, Moisen G, Czaplewski R (eds) Forest Inventory and Analysis (FIA) Symposium 2008; October 21-23, 2008. Park City, UT. Proceedin. *USDA Forest Service Proceedings - RMRS-P-56*, 1–26.

Houghton, R. A., Hall, F., & Goetz, S. J. (2009). Importance of biomass in the global carbon cycle. *Journal of Geophysical Research: Biogeosciences*, *114*(3). https://doi.org/10.1029/2009JG000935

Huston, M. A., & Wolverton, S. (2009). The global distribution of net primary production: Resolving the paradox. *Ecological Monographs*, *79*(3), 343–377. https://doi.org/10.1890/08-0588.1

Irving, A. D., Connell, S. D., & Russell, B. D. (2011). Restoring coastal plants to improve global carbon storage: Reaping what we sow. *PLoS ONE*, *6*(3). https://doi.org/10.1371/journal.pone.0018311

James, S. A., Meinzer, F. C., Goldstein, G., Woodruff, D., Jones, T., Restom, T., Mejia, M., Clearwater, M., & Campanello, P. (2003). Axial and radial water transport and internal water storage in tropical forest canopy trees. *Oecologia*, *134*(1), 37–45. https://doi.org/10.1007/s00442-002-1080-8

Jenkins, J. C., Chojnacky, D. C., Heath, L. S., & Birdsey, R. A. (2003). National-scale biomass estimators for United States tree species. *Forest Science, 49*(1), 12–35. https://doi.org/10.1093/forestscience/49.1.12

Jia, G., Shevliakova, E., Noblet-Ducoudré, N. De, Houghton, R., House, J., Kitajima, K., Lennard, C., Popp, A., Sirin, A., Sukumar, R., & Verchot, L. (2019). Land–climate interactions. In P. Bernier, J. C. Espinoza, & S. Semenov (Eds.), *Climate Change and Land: an IPCC special report on climate change, desertification, land degradation, sustainable land management, food security, and greenhouse gas fluxes in terrestrial ecosystems*. https://doi.org/10.1017/9781009157988.004

Kauffman, J. B., Giovanonni, L., Kelly, J., Dunstan, N., Borde, A., Diefenderfer, H., Cornu, C., Janousek, C., Apple, J., & Brophy, L. (2020). Total ecosystem carbon stocks at the marine-terrestrial interface: Blue carbon of the Pacific Northwest Coast, United States. *Global Change Biology*, *26*(10), 5679–5692. https://doi.org/10.1111/gcb.15248

Kelleway, J. J., Adame, M. F., Gorham, C., Bratchell, J., Serrano, O., Lavery, P. S., Owers, C. J., Rogers, K., Nagel-Tynan, Z., & Saintilan, N. (2021). Carbon storage in the coastal swamp oak forest wetlands of Australia. In *Wetland Carbon and Environmental Management* (pp. 339–353). Wiley. https://doi.org/10.1002/9781119639305.ch18

Kitin, P., Fujii, T., Abe, H., & Takata, K. (2009). Anatomical features that facilitate radial flow across growth rings and from xylem to cambium in *Cryptomeria japonica*. *Annals of Botany, 103*(7), 1145–1157. https://doi.org/10.1093/aob/mcp050

Komatsu, H., Kume, T., & Shinohara, Y. (2017). Optimal sap flux sensor allocation for stand transpiration estimates: A non-dimensional analysis. *Annals of Forest Science, 74*(2). https://doi.org/10.1007/s13595-017-0638-x

Kotowska, M. M., Link, R. M., Röll, A., Hertel, D., Hölscher, D., Waite, P. A., Moser, G., Tjoa, A., Leuschner, C., & Schuldt, B. (2021). Effects of wood hydraulic properties on water use and [roductivity of tropical rainforest trees. *Frontiers in Forests and Global Change*, *3*. https://doi.org/10.3389/ffgc.2020.598759

Krauss, K. W., & Duberstein, J. A. (2010). Sapflow and water use of freshwater wetland trees exposed to saltwater incursion in a tidally influenced South Carolina watershed. *Canadian Journal of Forest Research*, *40*(3), 525–535. https://doi.org/10.1139/x09-204

Krauss, K. W., Duberstein, J. A., & Conner, W. H. (2015). Assessing stand water use in four coastal wetland forests using sapflow techniques: Annual estimates, errors and associated uncertainties. *Hydrological Processes*, *29*(1), 112–127. https://doi.org/10.1002/hyp.10130

Krauss, K. W., Doyle, T. W., Twilley, R. R., Smith, T. J., Whelan, K. R. T., & Sullivan, J. K. (2005). Woody Debris in the mangrove forests of South Florida. *Biotropica*, *37*(1), 9–15. https://doi.org/10.1111/j.1744-7429.2005.03058.x

Krauss, K. W., Duberstein, J. A., Doyle, T. W., Conner, W. H., Day, R. H., Inabinette, L. W., Whitbeck, J. L., Krauss, A., Ken, W., Jamie, A., Thomas, W., William, H., & Richard, H. (2009). Site condition, structure, and growth of baldcypress along tidal/non-tidal salinity gradients. *Wetlands*, *29*(2), 505–519. https://doi.org/10.1672/08-77.1

Krauss, K. W., Noe, G. B., Duberstein, J. A., Conner, W. H., Stagg, C. L., Cormier, N., Jones, M. C., Bernhardt, C. E., Graeme Lockaby, B., From, A. S., Doyle, T. W., Day, R. H., Ensign, S. H., Pierfelice, K. N., Hupp, C. R., Chow, A. T., & Whitbeck, J. L. (2018). The role of the upper tidal estuary in wetland blue carbon storage and flux. *Global Biogeochemical Cycles*, *32*(5), 817–839. https://doi.org/10.1029/2018GB005897

Kume, T., Otsuki, K., Du, S., Yamanaka, N., Wang, Y. L., & Liu, G. Bin. (2012). Spatial variation in sap flow velocity in semiarid region trees: Its impact on stand-scale transpiration estimates. *Hydrological Processes*, *26*(8), 1161–1168. https://doi.org/10.1002/hyp.8205

Kwan, V., Fong, J., Ng, C. S. L., & Huang, D. (2022). Temporal and spatial dynamics of tropical macroalgal contributions to blue carbon. *Science of the Total Environment, 828*. https://doi.org/10.1016/j.scitotenv.2022.154369

Laffoley, D. (2009). *The Management of Natural Coastal Carbon Sinks.* Laffoley, D. & Grimsditch, G. D. (Eds.). IUCN.

Laffoley, D., & Grimsditch, G. (2009). *The management of natural coastal carbon sinks*. IUCN. http://admin.indiaenvironmentportal.org.in/files/carbon_managment_report_final_printed_version_1.pdf#page=57

Landsberg, J., & Waring, R. (2017). Water relations in tree physiology: Where to from here? *Tree Physiology*, *37*(1), 18–32. https://doi.org/10.1093/treephys/tpw102

Lascano, R. J., Goebel, T. S., Booker, J., Baker, J. T., & Gitz III, D. C. (2016). The stem heat balance method to measure transpiration: Evaluation of a new sensor. *Agricultural Sciences*, *07*(09), 604–620. https://doi.org/10.4236/as.2016.79057

Lininger, K. B., Wohl, E., Sutfin, N. A., & Rose, J. R. (2017). Floodplain downed wood volumes: a comparison across three biomes. *Earth Surface Processes and Landforms*, *42*(8), 1248–1261. https://doi.org/10.1002/esp.4072

Liu, X., Conner, W. H., Song, B., & Jayakaran, A. D. (2017). Forest composition and growth in a freshwater forested wetland community across a salinity gradient in South Carolina, USA. *Forest Ecology and Management*, *389*, 211–219. https://doi.org/10.1016/j.foreco.2016.12.022

Lovelock, C. E., & Duarte, C. M. (2019). Dimensions of blue carbon and emerging perspectives. In *Biology Letters* (Vol. 15, Issue 3). Royal Society Publishing. https://doi.org/10.1098/rsbl.2018.0781

Lu, P., Laurent, U., & Zhao, P. (2004). Granier's thermal dissipation probe (TDP) method for measuring sap flow in trees: Theory and practice. *Acta Botanica Sinica*, *46*(6), 631–646.

MacDicken, K. G. (2015). Global forest resources assessment 2015: What, why and how? *Forest Ecology and Management*, *352*, 3–8. https://doi.org/10.1016/J.FORECO.2015.02.006

Maltese, A., Awada, H., Capodici, F., Ciraolo, G., Loggia, G. La, & Rallo, G. (2018). On the use of the eddy covariance latent heat flux and sap flow transpiration for the validation of a surface energy balance model. *Remote Sensing*, *10*(2). https://doi.org/10.3390/rs10020195

McLeod, E., Chmura, G. L., Bouillon, S., Salm, R., Björk, M., Duarte, C. M., Lovelock, C. E., Schlesinger, W. H., & Silliman, B. R. (2011). A blueprint for blue carbon: Toward an improved understanding of the role of vegetated coastal habitats in sequestering CO2. *Frontiers in Ecology and the Environment*, *9*(10), 552–560. https://doi.org/10.1890/110004

Merlin, M., Solarik, K. A., & Landhäusser, S. M. (2020). Quantification of uncertainties introduced by data-processing procedures of sap flow measurements using the cut-tree method on a large mature tree. *Agricultural and Forest Meteorology*, *287*. https://doi.org/10.1016/j.agrformet.2020.107926

Molina, A. J., Aranda, X., Carta, G., Llorens, P., Romero, R., Savé, R., & Biel, C. (2016). Effect of irrigation on sap flux density variability and water use estimate in cherry (Prunus avium) for timber production: Azimuthal profile, radial profile and sapwood estimation. *Agricultural Water Management*, *164*, 118–126. https://doi.org/10.1016/j.agwat.2015.08.019

Nadezhdina, N., ˇCermák, J., & Nadezhdin, V. (1998). Heat field deformation method for sap flow measurements. In J. ˇCermák & N. Nadezhdina (Eds.), *Proceedings of the 4th International Workshop on Measuring Sap Flow in Intact Plants* (pp. 72–92). Publishing House of Mendel University.

Nelleman, C., Corcoran, E., Duarte, C. M., Valdes, L., DeYoung, C., Fonesca, L., & Grimsditch, G. (2009). *Blue Carbon. The Role of Healthy Oceans in Binding Carbon*. United Nations Environment Programme. www.grida.no

Noe, G. B., Hupp, C. R., Bernhardt, C. E., & Krauss, K. W. (2016). Contemporary deposition and long-term accumulation of sediment and nutrients by tidal freshwater forested wetlands impacted by sea level rise. *Estuaries and Coasts*, *39*(4), 1006–1019. https://doi.org/10.1007/s12237-016-0066-4

Noshiro, S., & Baas, P. (1998). Systematic wood anatomy of Cornaceae and Allies. *IAWA Journal*, *19*(1), 43–97.

Oishi, A. C., Hawthorne, D. A., & Oren, R. (2016). Baseliner: An open-source, interactive tool for processing sap flux data from thermal dissipation probes. *SoftwareX*, *5*, 139–143. https://doi.org/10.1016/j.softx.2016.07.003

Oishi, A. C., Oren, R., & Stoy, P. C. (2008). Estimating components of forest evapotranspiration: A footprint approach for scaling sap flux measurements. *Agricultural and Forest Meteorology*, *148*(11), 1719–1732. https://doi.org/10.1016/j.agrformet.2008.06.013

Oki, T., & Kanae, S. (2006). Global hydrological cycles and world water resources. *New Series*, *313*(5790), 1068–1072. https://www.jstor.org/stable/3847070

Oliveras, I., & Llorens, P. (2001). Medium-term sap flux monitoring in a Scots pine stand: A analysis of the operability of the heat dissipation method for hydrological purposes. *Tree Physiology*, *21*(7), 473–480. https://doi.org/10.1093/treephys/21.7.473

Oren, R., Phillips, N., Ewers, B. E., Pataki, D. E., & Megonigal, J. P. (1999). Sap-flux-scaled transpiration responses to light, vapor pressure deficit, and leaf area reduction in a flooded Taxodium distichum forest. *Tree Physiology*, *19*(6), 337–347. https://doi.org/10.1093/treephys/19.6.337

Oren, R., Sperry, J. S., Ewers, B. E., Pataki, D. E., Phillips, N., & Megonigal, J. P. (2001). Sensitivity of mean canopy stomatal conductance to vapor pressure deficit in a flooded Taxodium distichum L. forest: Hydraulic and non-hydraulic effects. *Oecologia*, *126*(1), 21–29. https://doi.org/10.1007/s004420000497

Pan, Y., Birdsey, R. A., Fang, J., Houghton, R., Kauppi, P. E., Kurz, W. A., Phillips, O. L., Shvidenko, A., Lewis, S. L., Canadell, J. G., Ciais, P., Jackson, R. B., Pacala, S. W., Mcguire, A. D., Piao, S., Rautiainen, A., Sitch, S., & Hayes, D. (2011). A Large and persistent carbon sink in the world's forests. *Science*, *333*(6045), 988–993. https://doi.org/10.1126/science,1204588

Parkinson, R. W., & Wdowinski, S. (2023). Geomorphic response of the Georgia Bight coastal zone to accelerating sea level rise, southeastern USA. *Coasts*, *4*(1), 1–20. https://doi.org/10.3390/coasts4010001

Pendleton, L., Donato, D. C., Murray, B. C., Crooks, S., Jenkins, W. A., Sifleet, S., Craft, C., Fourqurean, J. W., Kauffman, J. B., Marbà, N., Megonigal, P., Pidgeon, E., Herr, D., Gordon, D., & Baldera, A. (2012). Estimating global "blue carbon" emissions from conversion and degradation of vegetated coastal ecosystems. *PLoS ONE*, *7*(9). https://doi.org/10.1371/journal.pone.0043542

Penman, Jim., Gytarsky, M., Hiraishi, T., Krug, T., Kruger, D., Pipatti, R., Buendia, L., Miwa, K., Ngara, T., Tanabe, K., & Wagner, F. (2003). *Good practice guidance for land use, land-use change and forestry*. Institute for Global Environmental Strategies (IGES).

Peters, R. L., Fonti, P., Frank, D. C., Poyatos, R., Pappas, C., Kahmen, A., Carraro, V., Prendin, A. L., Schneider, L., Baltzer, J. L., Baron-Gafford, G. A., Dietrich, L., Heinrich, I., Minor, R. L., Sonnentag, O., Matheny, A. M., Wightman, M. G., & Steppe, K. (2018). Quantification of uncertainties in conifer sap flow measured with the thermal dissipation method. *New Phytologist*, *219*(4), 1283–1299. https://doi.org/10.1111/nph.15241

Peters, R. L., Pappas, C., Hurley, A. G., Poyatos, R., Flo, V., Zweifel, R., Goossens, W., & Steppe, K. (2021). Assimilate, process and analyse thermal dissipation sap flow data using the TREX r package. *Methods in Ecology and Evolution*, *12*(2), 342–350. https://doi.org/10.1111/2041-210X.13524

Philip, J. R. (1966). Plant water relations: Some physical aspects. *Annual Review of Plant Physiology*, *17*, 245–268. https://www.annualreviews.org/doi/pdf/10.1146/annurev.pp.17.060166.001333

Poyatos, R., Cermak, J., & Llorens, P. (2007). Variation in the radial patterns of sap flux density in pubescent oak (*Quercus pubescens*) and its implications for tree and stand transpiration measurements. *Tree Physiology*, *27*(4), 537–548. https://doi.org/10.1093/treephys/27.4.537

Poyatos, R., Granda, V., Flo, V., Adams, M. A., Adorján, B., Aguadé, D., Aidar, M. P. M., Allen, S., Alvarado-Barrientos, M. S., Anderson-Teixeira, K. J., Aparecido, L. M., Altaf Arain, M., Aranda, I., Asbjornsen, H., Baxter, R., Beamesderfer, E., Berry, Z. C., Berveiller, D., Blakely, B., … Martínez-Vilalta, J. (2021). Global transpiration data from sap flow measurements: The SAPFLUXNET database. In *Earth System Science Data* (Vol. 13, Issue 6). https://doi.org/10.5194/essd-13-2607-2021

Poyatos, R., Granda, V., Molowny-Horas, R., Mencuccini, M., Steppe, K., & Martínez-Vilalta, J. (2016). SAPFLUXNET: Towards a global database of sap flow measurements. *Tree Physiology*, *36*(12), 1449–1455. https://doi.org/10.1093/treephys/tpw110

Pretzsch, H. (2019). The effect of tree crown allometry on community dynamics in mixed-species stands versus monocultures. A review and perspectives for modeling and silvicultural regulation. *Forests*, *10*(9). https://doi.org/10.3390/f10090810

Ren, R., Liu, G., Wen, M., Horton, R., Li, B., & Si, B. (2017). The effects of probe misalignment on sap flux density measurements and in situ probe spacing correction methods. *Agricultural and Forest Meteorology*, *232*, 176–185. https://doi.org/10.1016/j.agrformet.2016.08.009

Reyes-Acosta, J. L., Vandegehuchte, M. W., Steppe, K., & Lubczynski, M. W. (2012). Novel, cyclic heat dissipation method for the correction of natural temperature gradients in sap flow measurements. Part 2. Laboratory validation. *Tree Physiology*, *32*(7), 913–929. https://doi.org/10.1093/treephys/tps042

Ricker, M. C., Blosser, G. D., Conner, W. H., & Lockaby, B. G. (2019). Wood biomass and carbon pools within a floodplain forest of the Congaree River, South Carolina, USA. *Wetlands*, *39*(5), 1003–1013. https://doi.org/10.1007/s13157-019-01150-1

Rodell, M., Beaudoing, H. K., L'Ecuyer, T. S., Olson, W. S., Famiglietti, J. S., Houser, P. R., Adler, R., Bosilovich, M. G., Clayson, C. A., Chambers, D., Clark, E., Fetzer, E. J., Gao, X., Gu, G., Hilburn, K., Huffman, G. J., Lettenmaier, D. P., Liu, W. T., Robertson, F. R., … Wood, E. F. (2015). The observed state of the water cycle in the early twenty-first century. *Journal of Climate*, *28*(21), 8289–8318. https://doi.org/10.1175/JCLI-D-14-00555.1

Román-Jordán, E., Esteban, L. G., de Palacios, P., & Fernández, F. G. (2017). Comparative wood anatomy of the Cupressaceae and correspondence with phylogeny, with special reference to the monotypic taxa. *Plant Systematics and Evolution*, *303*(2), 203–219. https://doi.org/10.1007/s00606-016-1364-9

Rozendaal, D. M. A., Requena Suarez, D., De Sy, V., Avitabile, V., Carter, S., Adou Yao, C. Y., Alvarez-Davila, E., Anderson-Teixeira, K., Araujo-Murakami, A., Arroyo, L., Barca, B., Baker, T. R., Birigazzi, L., Bongers, F., Branthomme, A., Brienen, R. J. W., Carreiras, J. o. M. B., Cazzolla Gatti, R., Cook-Patton, S. C., … Herold, M. (2022). Aboveground forest biomass varies across continents, ecological zones and successional stages: Refined IPCC default values for tropical and subtropical forests. *Environmental Research Letters*, *17*(1). https://doi.org/10.1088/1748-9326/ac45b3

Safwan Azman, M., Sharma, S., Liyana Hamzah, M., Mohamad Zakaria, R., Palaniveloo, K., & MacKenzie, R. A. (2023). Total ecosystem blue carbon stocks and sequestration potential along a naturally regenerated mangrove forest chronosequence. *Forest Ecology and Management*, *527*. https://doi.org/10.1016/j.foreco.2022.120611

Santoro, M., Cartus, O., Carvalhais, N., Rozendaal, D. M. A., Avitabile, V., Araza, A., De Bruin, S., Herold, M., Quegan, S., Rodríguez-Veiga, P., Balzter, H., Carreiras, J., Schepaschenko, D., Korets, M., Shimada, M., Itoh, T., Moreno Martínez, Á., Cavlovic, J., Gatti, R. C., … Willcock, S. (2021). The global forest above-ground biomass pool for 2010 estimated from high-resolution satellite observations. *Earth System Science Data*, *13*(8), 3927–3950. https://doi.org/10.5194/essd-13-3927-2021

Sato, T., Oda, T., Igarashi, Y., Suzuki, M., & Uchiyama, Y. (2012). Circumferential sap flow variation in the trunks of Japanese cedar and cypress trees growing on a steep slope. *Hydrological Research Letters*, *6*(0), 104–108. https://doi.org/10.3178/hrl.6.104

Schlesinger, W. H., & Jasechko, S. (2014). Transpiration in the global water cycle. *Agricultural and Forest Meteorology*, *189–190*, 115–117. https://doi.org/10.1016/j.agrformet.2014.01.011

Shinohara, Y., Tsuruta, K., Ogura, A., Noto, F., Komatsu, H., Otsuki, K., & Maruyama, T. (2013). Azimuthal and radial variations in sap flux density and effects on stand-scale transpiration estimates in a Japanese cedar forest. *Tree Physiology*, *33*(5), 550–558. https://doi.org/10.1093/treephys/tpt029

Shukla, P. R., Skea, J., Calvo Buendia, E., Masson-Delmotte, V., Pörtner, H.-O., Roberts, D., Zhai, P., Slade, R., Connors, S., van Diemem, R., Ferrat, M., Haughey, E., Luz, S., Neogi, S., Pathak, M., Petzold, J., Portugal Pereira, J., Vyas, P., Huntley, E., … Malley. (2019). *Climate Change and Land: an IPCC special report on climate change, desertification, land degradation, sustainable land management, food security, and greenhouse gas fluxes in terrestrial ecosystems*. Cambridge University Press. https://doi.org/10.1017/9781009157988

Smith, P., Adams, J., Beerling, D. J., Beringer, T., Calvin, K. V, Fuss, S., Griscom, B., Hagemann, N., Kammann, C., Kraxner, F., Minx, J. C., Popp, A., Renforth, P., Luis, J., Vicente, V., & Keesstra, S. (2019). Land-management options for greenhouse gas removal and their impacts on ecosystem services and the sustainable development goals. *Annual Review of Environment and Resources*, *7*, 40. https://doi.org/10.1146/annurev-environ-101718

Spivak, A. C., Sanderman, J., Bowen, J. L., Canuel, E. A., & Hopkinson, C. S. (2019). Global-change controls on soil-carbon accumulation and loss in coastal vegetated ecosystems. *Nature Geoscience*, *12*(9), 685–692. https://doi.org/10.1038/s41561-019-0435-2

Steppe, K., De Pauw, D. J. W., Doody, T. M., & Teskey, R. O. (2010). A comparison of sap flux density using thermal dissipation, heat pulse velocity and heat field deformation methods. *Agricultural and Forest Meteorology*, *150*(7–8), 1046–1056. https://doi.org/10.1016/j.agrformet.2010.04.004

Stuckey, B. N. (1982). *Soil Survey of Georgetown County South Carolina*. United States Department of Agriculture Soil Conservation Service.

Tsuruta, K., Kume, T., Komatsu, H., Higashi, N., Umebayashi, T., Kumagai, T., & Otsuki, K. (2010). Azimuthal variations of sap flux density within Japanese cypress xylem trunks and their effects on tree transpiration estimates. *Journal of Forest Research*, *15*(6), 398–403. https://doi.org/10.1007/s10310-010-0202-0

USDA Forest Service. (2019). *Forest Inventory and Analysis National Core Field Guide, volume 1, version 9.0*. *I*. http://fia.fs.fed.us/%5Cnlibrary/field-guides-methods-proc

Van Bavel, C. H. M., & Van Bavel, M. G. (1993). *Apparatus for Measuring Sap Flow* (Patent 5337604).

Van de Wal, B. A. E., Guyot, A., Lovelock, C. E., Lockington, D. A., & Steppe, K. (2015). Influence of temporospatial variation in sap flux density on estimates of whole-tree water use in *Avicennia marina*. *Trees - Structure and Function*, *29*(1), 215–222. https://doi.org/10.1007/s00468-014-1105-z

Van Wagner C.E. (1968). The line intersect method in forest fuel sampling. *Forest Science*, *14*(1), 20–26.

Vandegehuchte, M. W., & Steppe, K. (2013). Sap-flux density measurement methods: Working principles and applicability. *Functional Plant Biology*, *40*(10), 1088. https://doi.org/10.1071/fp12233_co

Vorster, A. G., Evangelista, P. H., Stovall, A. E. L., & Ex, S. (2020). Variability and uncertainty in forest biomass estimates from the tree to landscape scale: The role of allometric equations. *Carbon Balance and Management*, *15*(1), 1–20. https://doi.org/10.1186/s13021-020-00143-6

Wang, H., Dai, Z., Trettin, C. C., Krauss, K. W., Noe, G. B., Burton, A. J., Stagg, C. L., & Ward, E. J. (2022). Modeling impacts of drought-induced salinity intrusion on carbon dynamics in tidal freshwater forested wetlands. *Ecological Applications*, *32*(8), 1–16. https://doi.org/10.1002/eap.2700

Ward, E. J., Domec, J. C., King, J., Sun, G., McNulty, S., & Noormets, A. (2017). TRACC: an open source software for processing sap flux data from thermal dissipation probes. *Trees - Structure and Function*, *31*(5), 1737–1742. https://doi.org/10.1007/s00468-017-1556-0

Ward, E. J., Domec, J. C., Laviner, M. A., Fox, T. R., Sun, G., McNulty, S., King, J., & Noormets, A. (2015). Fertilization intensifies drought stress: Water use and stomatal conductance of *Pinus taeda* in a midrotation fertilization and throughfall reduction experiment. *Forest Ecology and Management*, *355*, 72–82. https://doi.org/10.1016/j.foreco.2015.04.009

Wiedemann, A., Marañón-Jiménez, S., Rebmann, C., Herbst, M., & Cuntz, M. (2016). An empirical study of the wound effect on sap flux density measured with thermal dissipation probes. *Tree Physiology*, *36*(12), 1471–1484. https://doi.org/10.1093/treephys/tpw071

Wilson, K. B., Hanson, P. J., Mulholland, P. J., Baldocchi, D. D., & Wullschleger, S. D. (2001). A comparison of methods for determining forest evapotranspiration and its components: Sap-flow, soil water budget, eddy covariance and catchment water balance. *Agricultural and Forest Meteorology*, *106*(2), 153–168. https://doi.org/10.1016/S0168-1923(00)00199-4

Woodall, C. W., Heath, L. S., Domke, G. M., & Nichols, M. C. (2011). Methods and equations for estimating aboveground volume, biomass, and carbon for trees in the U.S. forest inventory, 2010. *General Technical Report NRS-88*.

Zon, R., & Sparhawk, W. N. (1923). *Forest Resources of the World* (First Edition). McGraw-Hill Book Co. Inc.